Wind and Structures, *Vol. 21, No. 2 (2015) 119-158*
DOI: http://dx.doi.org/10.12989/was.2015.21.2.119

Vertical coherence functions of wind forces and influences on wind-induced responses of a high-rise building with section varying along height

D.M. Huang*[1,3], L.D. Zhu[2a], W. Chen[2b] and Q.S. Ding[2c]

[1]*School of Civil Engineering, Central South University, Changsha 410075, China*
[2]*State Key Laboratory for Disaster Reduction in Civil Engineering, Tongji University, Shanghai 200092, China*
[3]*National Engineering Laboratory for High Speed Railway Construction, Central South University, Changsha 410075, China*

(Received January 24, 2015, Revised February 13, 2015, Accepted March 26, 2015)

Abstract. The characteristics of the coherence functions of X axial, Y axial, and RZ axial (i.e., body axis) wind forces on the Shanghai World Trade Centre - a 492 m super-tall building with section varying along height are studied via a synchronous multi-pressure measurement of the rigid model in wind tunnel simulating of the turbulent, and the corresponding mathematical expressions are proposed there from. The investigations show that the mathematical expressions of coherence functions in across-wind and torsional-wind directions can be constructed by superimposition of a modified exponential decay function and a peak function caused by turbulent flow and vortex shedding respectively, while that in along-wind direction need only be constructed by the former, similar to that of wind speed. Moreover, an inductive analysis method is proposed to summarize the fitted parameters of the wind force coherence functions of every two measurement levels of altitudes. The comparisons of the first three order generalized force spectra show that the proposed mathematical expressions accord with the experimental results well. Later, the influences of coherence functions on wind-induced dynamic responses are analyzed in detail based on the proposed mathematical expressions and the frequency-domain method of random vibration theory.

Keywords: high-rise building; wind tunnel test for pressure measurement; coherence function; mathematical expressions; parameter fitting; peak function; inductive analysis method

1. Introduction

With the development of modern materials and construction techniques, a number of skyscrapers with unique shapes have been constructed. And with the height and flexibility of buildings increasing, the wind loads would bring about direct and critical influences on their safety and serviceability. Consequently, the precise determination of wind loads is an outstanding and crucial issue.

*Corresponding author, E-mail: huangdongmei_tumu@163.com
[a] E-mail: ledong@tongji.edu.cn
[b] E-mail: chenwei@tongji.edu.cn
[b] E-mail: qsding@mail.tongji.edu.cn

http://www.techno-press.org/?journal=was&subpage=8 ISSN: 1226-6116 (Print), 1598-6225 (Online)

In the early stages, the determination of wind loads in the along-wind direction was on the basis of quasi-steady theory, which means that the power spectra and coherence functions of wind loads on structures were derived from that of wind speed (Simiu and Scanlan1996). In recent years, with the advances in synchronous multi-pressure measurement technology in wind tunnel tests, the non-steady aerodynamic forces of along-wind, across-wind and torsion-wind on buildings with various types of appearance are easily obtained, The corresponding power spectra and coherence functions of these wind forces can then be obtained. These advances make the wind loads and then the wind-induced responses more accurately. Moreover, to study the distinguishing features of non-steady aerodynamic forces deeply and carry out some analysis on the wind-induced dynamic responses in detail, further investigations on the characteristics and the mathematical expressions of the power spectra and the coherence functions of non-steady aerodynamic forces are necessary.

For unsteady wind load spectra, detailed characteristics and mathematical expressions have been analyzed and proposed via high-frequency dynamic balance wind tunnel tests and synchronous multi-pressure measurement wind tunnel tests, not only in along-wind but also in across-wind and torsion-wind directions (Lin *et al.* 2005, Marukawa *et al.* 1992, Gu and Quan 2004, Liang *et al*. 2002, 2004). However, these mathematical expressions mainly focus on some buildings with typical cross-section unchanging along the height, but are not applicable to all buildings. Therefore, for the specific, irregular, cross-section changing along the height, high-rise buildings, special analyses are necessary based on wind tunnel simulation of the turbulent (Huang *et al*. 2014).

For the coherence functions of wind speed, several classical mathematical expressions have been widely used: an exponential decay function, which was related to frequency, distance, and mean wind speeds between two points considered, was proposed by Davenport (1965) and subsequently selected by China Load Code (GB 50009-2006); a simplified exponential decay function, which was related to only distance and average height of two points considered, was suggested by Shiotani and Iwatani(1972) and where after adopted by ECCS (1978); a modified exponential decay function, which was well coincide with the measured results of “head drop” at low frequencies (i.e., the coherence function is less than 1 when the reduced frequency is equal to zero.), was derived by Krenk (1995), and Hansen and Krenk (1999). However, for the coherence functions of unsteady wind loads, the outcomes rest only on their characteristic analysis but not on their mathematical expressions (Lin *et al.* 2005). Therefore, special and further investigations on characteristics and mathematical expressions of coherence functions of unsteady wind loads for regular and irregular high-rise buildings are essential.

As we all know, there are two principal approaches to the estimation of wind-induced responses without considering coherence function of wind loads: one is to utilize aerodynamic base moment/torque spectra (Kareem and Zhou 2003), which is a frequency domain approach based on the gust loading factor concept, the other is to use time history of pressure measurements directly in the time domain (Simiu *et al*. 2006, NIST HR-DAD). However, the above first approach can not consider the influences of higher modes and their coupling on wind-induced responses, and the second approach cannot shed light on the influences of vortex shedding on wind-induced responses in any detail for the turbulent force and vortex induced force in the time domain are difficult to be separated. Moreover, the correlation analyses of wind loads in the frequency domain can provide more information than that in the time domain. In addition to its theoretic value, the coherence function would be needed if the instantaneous pressure measurements on the entire building facade have to be done in groups with separate tests. In this case, the coherence functions can be used to combine these separately tested data for wind response analysis. Therefore, it is

necessary to analyze the characteristics, composition, and mathematical expressions for spectra and coherence functions of wind loads, and then to evaluate wind-induced responses in terms of random vibration theory in the frequency domain and analyze the influences of vortex shedding and other situations on wind-induced responses.

As we known, the power spectra and vertical coherence functions of wind loads are different from buildings with different appearances. However, their features and universal expressions, as well as the analytical method, share something in common. Moreover, the wind-induced responses of buildings in the frequency domain are related to the power spectrum matrix of wind loads, including auto-spectra and cross-spectra, which are relevant to auto-spectra and coherence functions when ignoring the influence of phase angles. In view of these, the characteristics of the coherence functions of wind forces on the Shanghai World Trade Centre, a famous and 492 m height super high-rise building having unique shape and varying cross-sections along height, should be studied by using the wind tunnel test for synchronization pressure measurement. And the corresponding mathematical expressions and their analytical method would be proposed follow. Subsequently, the influences of coherence functions on wind-induced dynamic responses would be analyzed in detail from the standpoint of the proposed mathematical expressions and the frequency-domain method of random vibration theory.

2. Wind tunnel test

2.1 Rigid model synchronization pressure measuring test

A synchronization pressure measurement test of the Shanghai World Trade Centre - a 492 m super high-rise building with varying section cross-along its height and an inverted trapezoid at its top part (as shown in Fig. 1) was conducted in the Atmospheric Boundary Layer Wind Tunnel, TJ-2, in Tongji University, China, with a working segment of 3 m in width, 2.5 m in height and 15m in length. The range of wind speed is from 1.0 m/s to 68 m/s. The wind filed in the atmospheric boundary layer was simulated mainly by spires, grid, and roughness elements. The simulated results of the mean wind speed profile, the along-wind and across-wind turbulence intensity profile, and the power spectra of along-wind and across-wind on gradient height are discussed in detail in Huang *et al.* (2014).

Fig. 1 Synchronous pressure measurement wind tunnel test of rigid model

The elevation profile, cross-sectional shapes of typical height, and measurement tap arrangement for this 492 m high-rise building are shown in Fig. 2 which show that the cross-sections of the building are close to a square at about layers 1 to 9, subsequently they have a pair of increasing corner cuts with increasing height and become an approximate rectangle with a 7.5:1 length-width ratio at the top; in addition, the cross-sections are separated into two parts at the upper most inverted trapezoid. Corresponding to a length scale ratio of 1:350, the total height of this model is 1.4 m. The test wind speed was 14 m/s, which was monitored at a reference level of 1.2 m in the wind tunnel, corresponding to gradient height of the atmospheric boundary layer, by a pitot tube (see Fig. 1). In total, 1,530 pressure measurement taps were distributed on 41 levels of altitude, which were numbered from bottom to top along the height of the model. Due to the limitations of the channels of the electronic scan valve, the signals of measuring taps could not be all collected simultaneously but were divided into four groups of A, B, C, and D , as shown in Fig. 2(b). Each pressure signal was sampled with 6,000 data points at a frequency of 312.5 Hz.

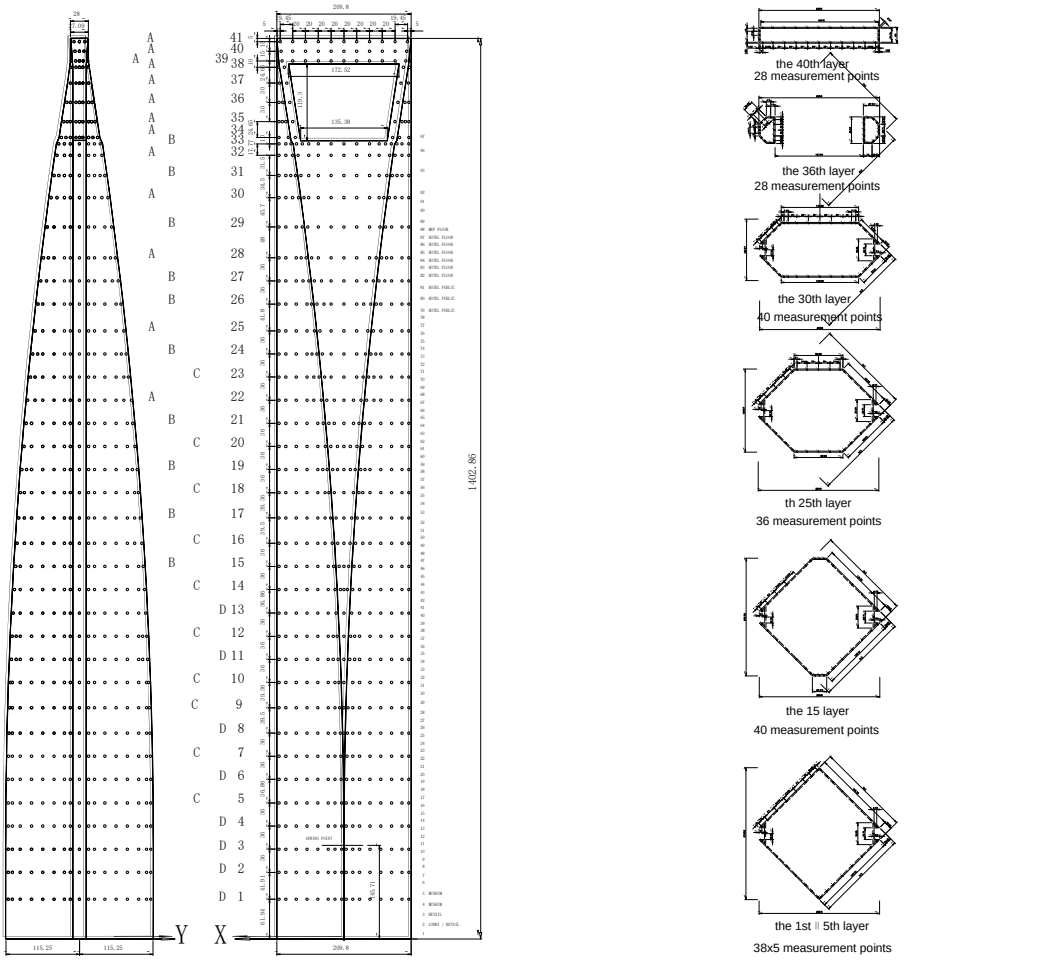

(a) side elevation (b) front elevation (c) cross-section on typical height

Fig. 2 Shape and measuring tap arrangement of façade and cross-sections of typical height

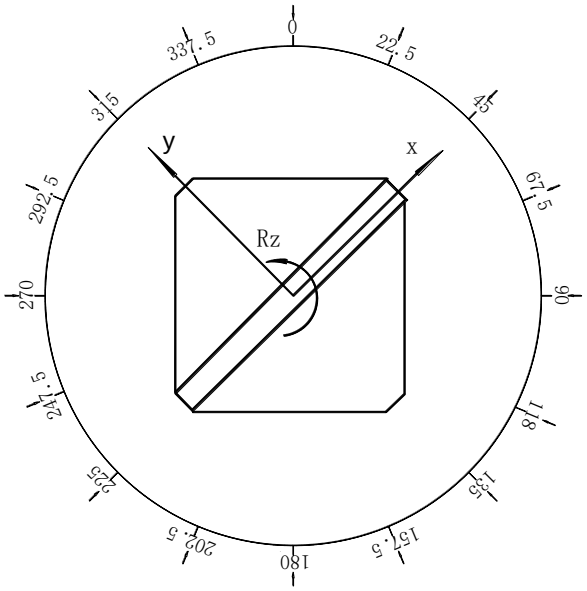

Fig. 3 Positions, wind directions and definitions of coordinate axes for the test model

The model orientation, wind direction and coordinate axes definitions are shown in Fig. 3, which can be understood by comparison with Fig. 2. The shape of the building is symmetrical about both X and Y-axes. In the wind directions of 315º and 135 º, the shape is also symmetrical about the along-wind direction and the across-wind direction, correspondingly, the Y direction of body-axis expresses the along-wind of wind field axis, the X direction of body-axis expresses the across-wind of wind field axis, and the RZ direction of body-axis expresses the torsion-wind of wind field axis. In the wind directions of 45º and 225º, the shape of building is also symmetrical about the along-wind direction and the across-wind direction, correspondingly, the X direction of body-axis expresses the along-wind of wind field axis, the Y direction of body-axis expresses the across-wind of wind field axis, and the RZ direction of body-axis expresses the torsion-wind of wind field axis. In other wind directions, the body-axes are not parallel or perpendicular to the wind field axes.

2.2 Aeroelastic model vibration measuring test

To compare the wind-induced responses based on the calculated and experimental results, an aeroelastic model test was also conducted in the TJ-2 Wind Tunnel at the same length scale of 1:350 (see Fig. 4); correspondingly, the design frequency scale was about 47:1, and the wind speed scale was 1:7.45. The test reference wind speeds were 2 m/s, 4 m/s, 6 m/s, 7 m/s, 8 m/s, and 9 m/s, monitored at a referenced height of 1.2m in wind tunnel. The corresponding prototype reference height is about 420 m, a little bit higher than the gradient height of the atmospheric boundary layer (i.e., 400 m as specified in the China Load Code for Type C terrain). To measure the static and dynamic displacement responses of the high-rise building's aeroelastic model, every three laser displacement sensors are placed on three different sections at heights of 1.38 m, 1.06 m, and 0.70

m (see Fig. 4). Of the three sensors, one measure the responses in the X-direction, the other two do so in the Y-direction, so the displacements of X-direction, Y-direction, and around-Z-direction can be obtained. During testing the sampling frequency of displacement signals is 200Hz and 12,288 samples were collected. The computed fundamental natural frequencies of the prototype building, and the identified fundamental natural frequencies and modal damping ratios of the aeroelastic model are listed in Table 1 (as investigated by Huang *et al*. (2008)).The first three computed structural modes of the prototype building and the identified results from the aeroelastic model are shown in Fig. 5.

Fig. 4 Aeroelastic model wind tunnel test

Table 1 Modal parameters: prototype and model

Mode	f_p(Hz)	f_m (HZ)	ω_m (rad/s)	ξ_m (%)
1st Bending along X-axis	0.156	7.38	46.3	0.28
2nd Bending along Y-axis	0.185	8.56	57.8	0.25
3rd Torsion around Z-axis	0.361	17.25	108.3	0.31

(Note: subscript *p* indicates prototype, and subscript *m* indicates model)

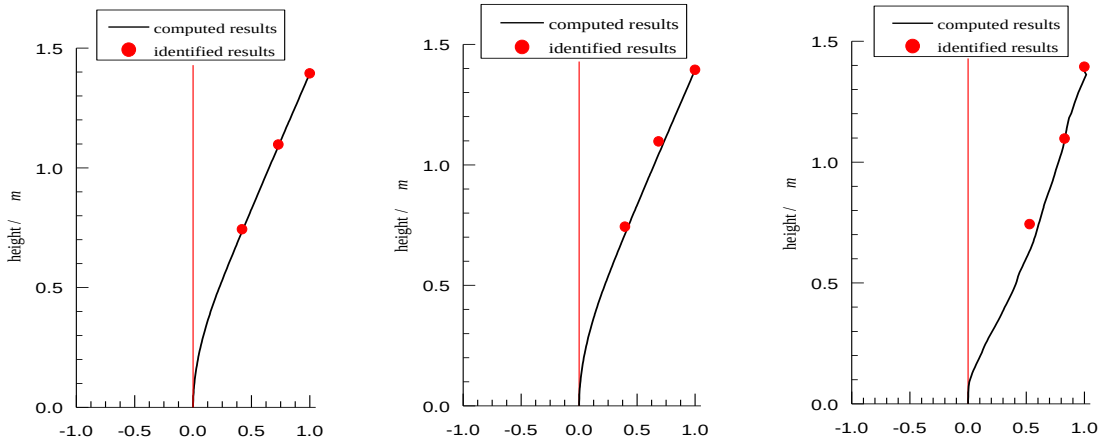

Fig. 5 First three structural circular frequencies and normalized mode shapes of computed and identified results

3. Characteristics of coherence functions of wind forces at different levels of altitude

As we all know, the dynamic FEM model of tall building is generally simplified as a series of rigid-floor model. Therefore, the wind loads on such structure are a series of concentrated forces acting on structural floors. According to random vibration theory in frequency domain, the wind-induced dynamic responses are related to the power spectra and coherence functions of the wind forces. The characteristics and the mathematical expressions of the power spectra of the wind forces were investigated in detail previously (Huang *et al*. 2014), the characteristics and mathematical expressions of the coherence functions of the wind forces are the focus of the research in this paper.

3.1 Time histories of wind force coefficients at different levels of altitude

In aerodynamics, the time-history of the dimensionless pressure coefficient on structural surfaces is expressed as follows

$$C_{ij}(t)=\frac{p_{ij}(t)-p_{r\infty}(t)}{p_{r0}(t)-p_{r\infty}(t)} \tag{1}$$

Where $C_{ij}(t)$ is the time-history of the dimensionless pressure coefficient of the j^{th} measuring tap at the i^{th} level of altitude, which takes the dynamic pressure at the reference point as its reference pressure; $p_{ij}(t)$ is the wind pressure time-history of the j^{th} measuring tap at the i^{th} level of altitude; $p_{r0}(t)$ and $p_{r\infty}(t)$ are the synchronously measured total pressure and static pressure time-histories at the reference point respectively ; $p_{r0}(t)-p_{r\infty}(t)$ expresses the dynamic pressure

time-history at the reference point.

To eliminate the distortions caused by the tubing system, the experimental (Irwin *et al.* 1979) and analytical (Holmes and Lewis 1987) methods were proposed. In this work, the wind pressures at each measuring tap are revised by the analytical method.

Subsequently, the time-histories of wind force coefficients at each measuring level can be calculated by the integral summation formulae:

$$C_{x_i}(t) = \sum_{j=1}^{m_i} C_{ij}(t) \cdot A_{ij} \cdot \cos(\alpha_{ij}) \cdot \sin(\beta_{ij}) / (B_{x_i} h_i) \tag{2a}$$

$$C_{y_i}(t) = \sum_{j=1}^{m_i} C_{ij}(t) \cdot A_{ij} \cdot \sin(\alpha_{ij}) \cdot \sin(\beta_{ij}) / (B_{y_i} h_i) \tag{2b}$$

$$C_{Rz_i}(t) = \sum_{j=1}^{m_i} \left[C_{ij}(t) \cdot A_{ij} \cdot \sin(\alpha_{ij}) \cdot \sin(\beta_{ij}) \cdot x_{ij} - C_{ij}(t) \cdot A_{ij} \cdot \cos(\alpha_{ij}) \cdot \sin(\beta_{ij}) \cdot y_{ij} \right] / (B_{x_i} B_{y_i} h_i) \tag{2c}$$

Where $C_{x_i}(t)$ 、 $C_{y_i}(t)$, and $C_{Rz_i}(t)$ are the time-histories of dimensionless wind force coefficients at the i^{th} measuring level along the X- and Y-axes, and around the Z-axis respectively; A_{ij} is the control area of the j^{th} measuring tap at the i^{th} level of altitude; α_{ij} is the angle (clockwise) between the projection in plane XOY of the surface normal at the j^{th} measuring tap at the i^{th} level of altitude and the X-axis; β_{ij} is the angle between the normal to the j^{th} measuring tap at the i^{th} level of altitude and the Z-axis; h_i is the effective height of the i^{th} measuring level of altitude; B_{x_i} and B_{y_i} are the characteristic widths at the i^{th} measuring level of altitude perpendicular to the X- and Y- axes respectively; x_{ij} and y_{ij} are the X- and Y- coordinates of the j^{th} measuring tap at the i^{th} level of altitude respectively; and m_i is the number of measuring taps at the i^{th}level of altitude.

3.2 Coherence functions of wind forces at different levels of altitude

The coherence function of wind forces can be defined as

$$\rho_{ab}(f) = \frac{|S_{ab}(f)|}{\sqrt{S_{aa}(f) \cdot S_{bb}(f)}} \tag{3}$$

where *a* and *b* express the two different positions; $S_{aa}(f)$ and $S_{bb}(f)$ are the auto-power spectra of wind forces at positions *a* and *b*, respectively; $S_{ab}(f)$ is the cross-power spectrum of the wind forces at positions *a* and *b*.

The wind force coefficients along the body-axes, as derived from integral summation formulae, are convenient for wind-induced responses analysis, however, that in the wind field axis directions are suitable for characteristics analysis of wind loads. The body-axis and the wind field axis have a corresponding conversion relationship. As mentioned, the shape of the building is symmetrical about the X- and Y-axes. Therefore, the investigations on characteristics of wind forces are focused

on wind directions 315°, 0°, and 45°. In the wind direction of 315°, the Y direction of body-axis expresses the along-wind of wind field axis, the X direction of body-axis expresses the across-wind of wind field axis, and the RZ direction of body-axis expresses the torsion-wind of wind field axis. In the wind direction of 45°, the X direction of body-axis expresses the along-wind of wind field axis, the Y direction of body-axis expresses the across-wind of wind field axis, and the RZ direction of body-axis expresses the torsion-wind of wind field axis. In the wind direction of 0°, the body-axes of X and Y directions are not parallel or perpendicular to the wind field axes. As seen in Fig. 2, the measuring taps of groups A and C groups nearly cover the entire building from top to bottom, therefore, the characteristic analysis of the coherence functions of wind forces would mainly adopt the data from these two groups.

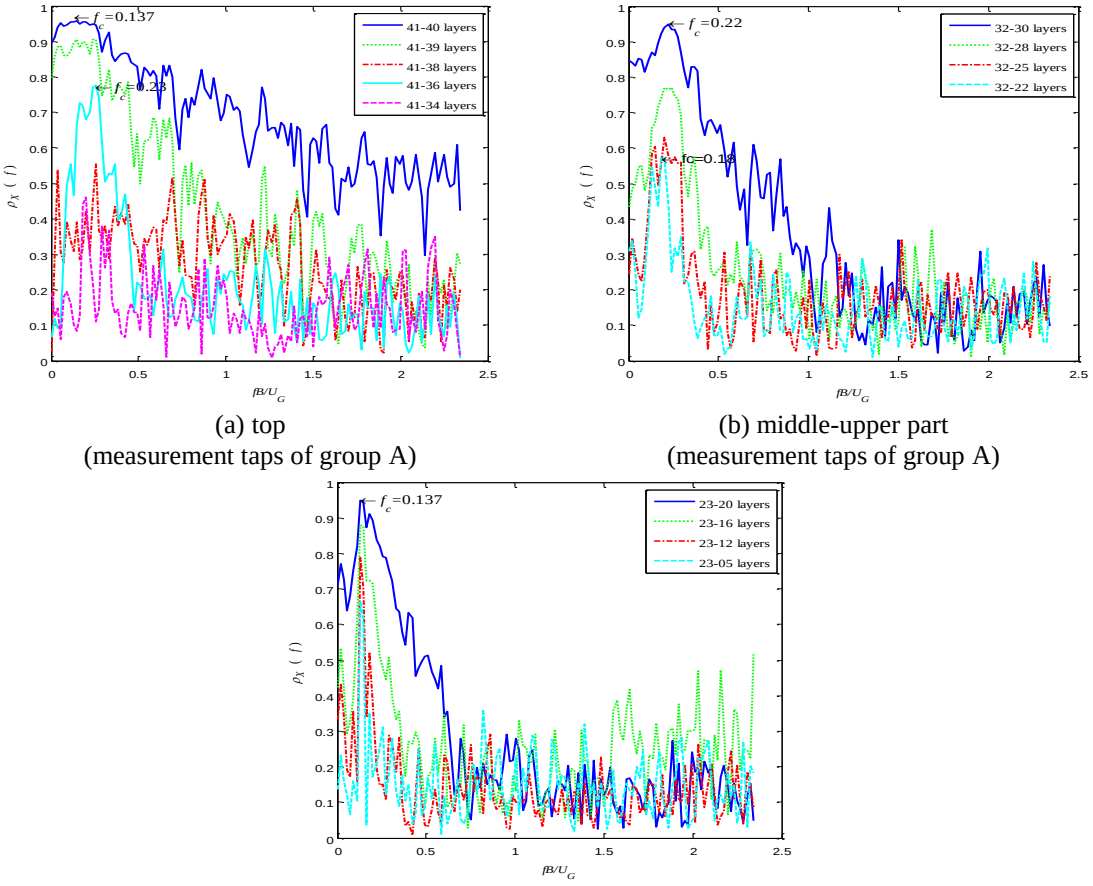

(a) top
(measurement taps of group A)

(b) middle-upper part
(measurement taps of group A)

(c) middle-lower part
(measurement taps of group C)

Fig. 6 Coherence functions of wind force coefficients along X-axis (across-wind) in wind direction 315°

(Note: $f_c = fB/U_G$ is the reduced frequency; B is the characteristics width perpendicular to the Y-axis; U_G is the gradient wind speed)

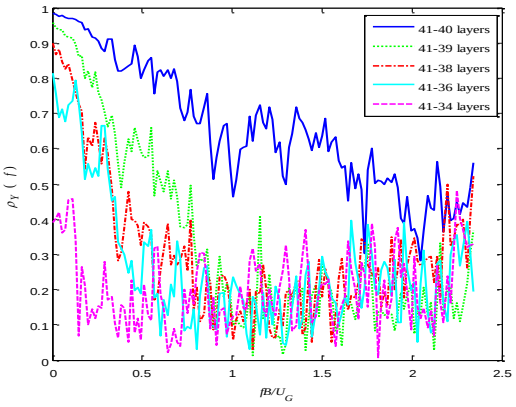

(a) top
(measurement taps of group A)

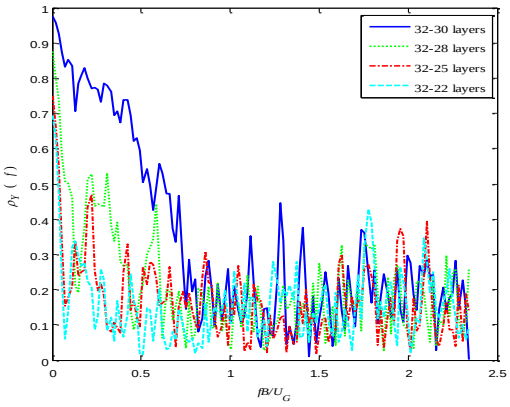

(b) middle-upper part
(measurement taps of group A)

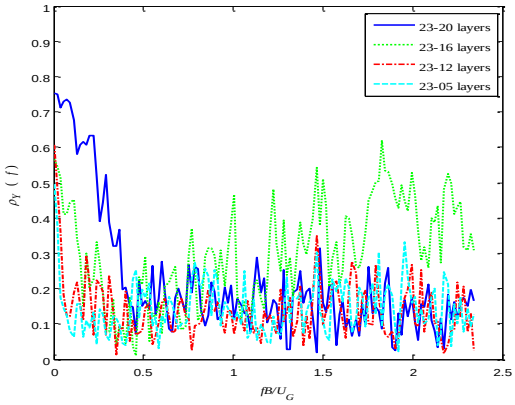

(c) middle-lower part
(measurement taps of group C)

Fig. 7 Coherence functions of wind force coefficients along Y-axis (along-wind) in wind direction 315°

(Note: $f_c = fB/U_G$ is the reduced frequency; B is the characteristics width perpendicular to the Y-axis; U_G is the gradient wind speed)

3.2.1 Wind direction 315°

Figs. 6 to 8 show the coherence functions of wind forces at different levels of altitude in the X-axis (across-wind), Y-axis (along-wind), and RZ-axis (torsional-wind) for wind direction of 315°, respectively, including different positions and different distances. These figures show that the coherence functions would become small if the distances between levels of altitude become larger. Furthermore, as shown in Fig. 6, the coherence functions in the X-axis (across-wind) obviously have peaks near the vortex shedding frequency, except that at the opening edge such as measurement levels of 34 and 38. This imply that the correlation of vortex-excited forcesappearslarger than that of turbulent flow force. At the top and upper parts of the structure, the reduced frequencies corresponding to these peaks are in range 0.18 to 0.23, and in the lower part of the structure, the reduced frequencies corresponding to such peaks are near 0.137. In the

case of similar inter-level distances, the peak becomes more obvious and narrow-banded with the decrement of the structural height. As shown in Fig. 7, the wind force coherence functions along Y-axis (along-wind) are similar to that of the wind speeds. As seen in Fig. 8, the coherence functions of the RZ-axis (torsional-wind) are similar to that of the X-axis (across-wind).At the top and the upper part of the structure, the reduced frequencies corresponding to such peaks are about 0.17, and in the lower part of the structure, the reduced frequencies corresponding to such peaks are near 0.137.

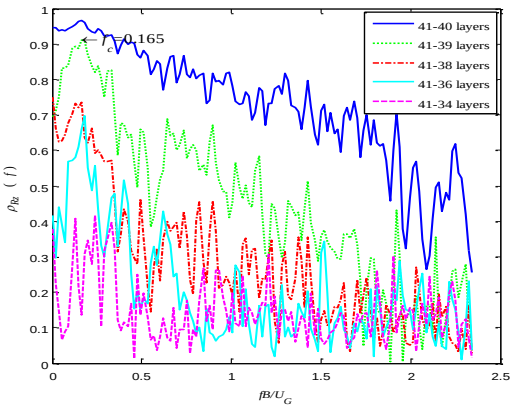

(a) top
(measurement taps of group A)

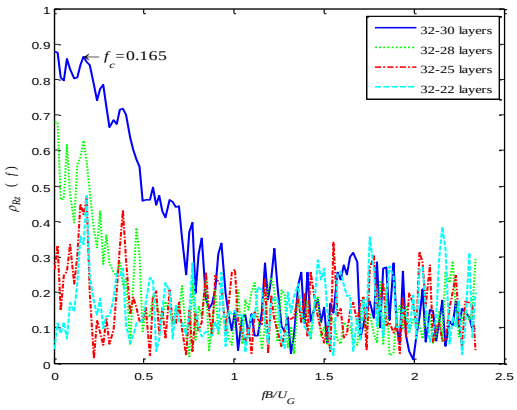

(b) middle-upper part
(measurement taps of group A)

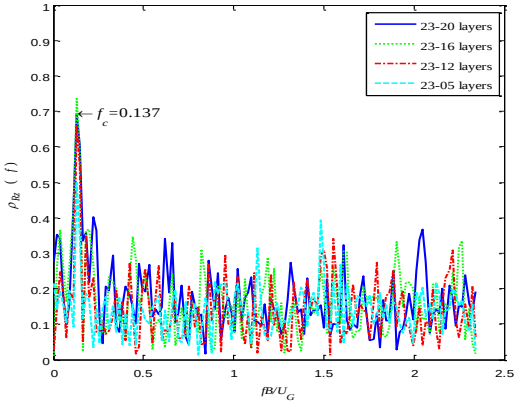

(c) middle-lower part
(measurement taps of group C)

Fig. 8 Coherence functions of wind force coefficients around Z-axis (torsional-wind) in wind direction 315°

(Note: $f_c = fB/U_G$ is the reduced frequency; B is the characteristics width perpendicular to the Y-axis; U_G is the gradient wind speed)

3.2.2 Wind direction 0º

Figs. 9 to 11 show the coherence functions of wind forces at different levels of altitude along the X axis (the angle between the X axis and along-wind direction or across-wind direction is 45º), Y-axis, and RZ-axis (torsional-wind) for wind direction of 0º, respectively, including different positions and different distances. These figures show that the coherence functions of wind forces along the X-axis, Y-axis and RZ-axis would become small if the distances between levels of altitude increase; furthermore, they have obvious peaks near the vortex shedding frequency except in the case of the opening and edge at the top. The reduced frequencies of peaks along the X and Y axes are about 0.2. However, those around the Z-axis have no obvious regularity.

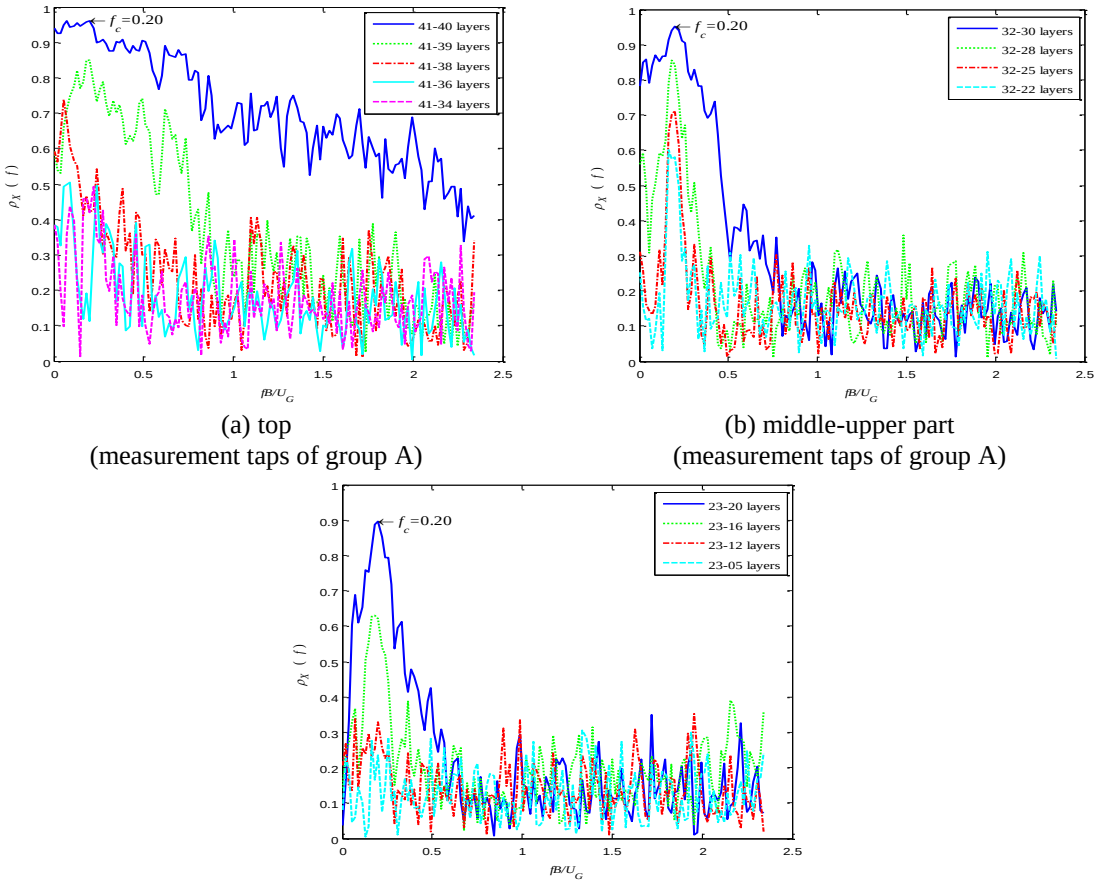

(a) top
(measurement taps of group A)

(b) middle-upper part
(measurement taps of group A)

(c) middle-lower part
(measurement taps of group C)

Fig. 9 Coherence functions of wind force coefficients along X-axis in wind direction 0°

Note: $f_c = fB/U_G$ is the reduced frequency; B is the characteristics width perpendicular to the Y-axis; U_G is the gradient wind speed)

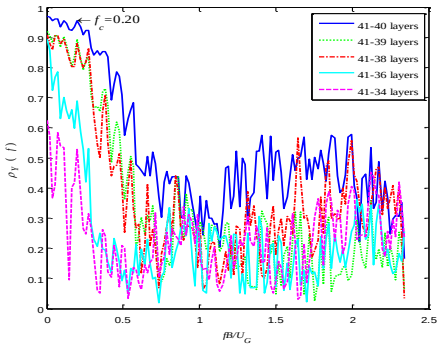

(a) top
(measurement taps of group A)

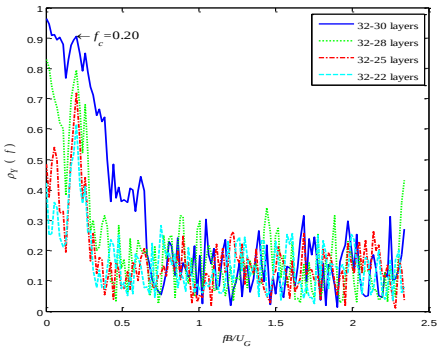

(b) middle-upper part
(measurement taps of group A)

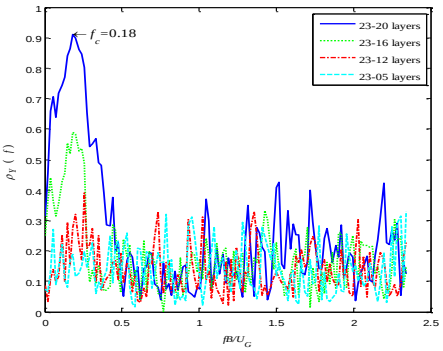

(c) middle-lower part
(measurement taps of group C)

Fig. 10 Coherence functions of wind force coefficients along Y-axis in wind direction 0^o

(Note: $f_c = fB/U_G$ is reduced frequency; B is characteristics width perpendicular to the Y-axis; U_G is the gradient wind speed)

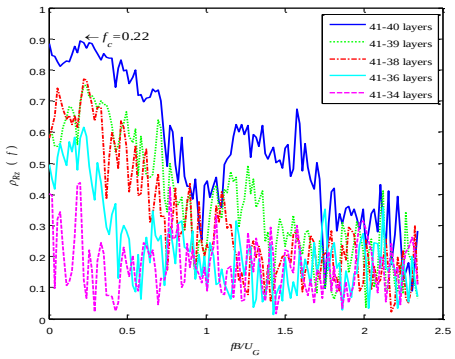

(a) top
(measurement taps of group A)

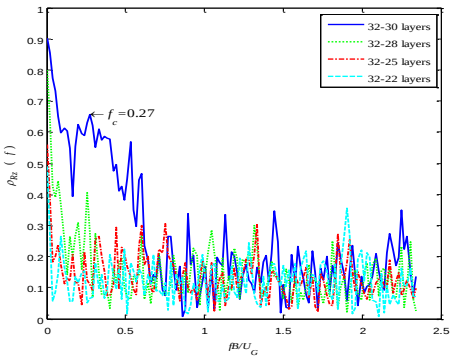

(b) middle-upper part
(measurement taps of group A)

Continued-

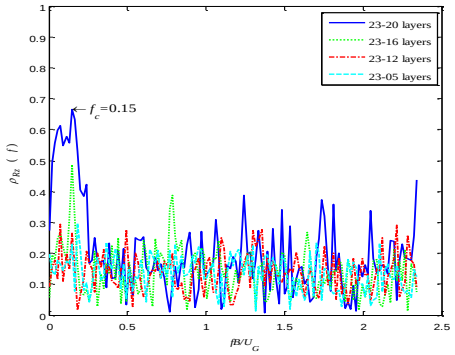

(c) middle-lower part
(measurement taps of group C)

Fig. 11 Coherence functions of wind force coefficients around Z-axis (torsional-wind) in wind direction 0°

(Note: $f_c = fB/U_G$ is the reduced frequency; B is the characteristics width perpendicular to the Y-axis; U_G is the gradient wind speed)

3.2.3 Wind direction 45°

Figs. 12 to 14 show the coherence functions of wind forces at different levels of altitude along the X-axis (along-wind), Y-axis (across-wind), and around the Z-axis (torsional-wind) for wind direction of 45°, respectively, including different positions and different distances. The coherence functions would diminish if the distances between levels of altitude increase. Furthermore, as shown in Fig. 12, the coherence functions of wind forces along the X-axis (along-wind) obey exponential decay laws, similar to that of the wind speeds.

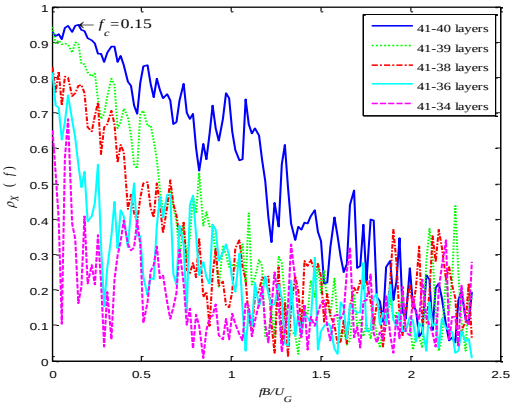

(a) top
(measurement taps of group A)

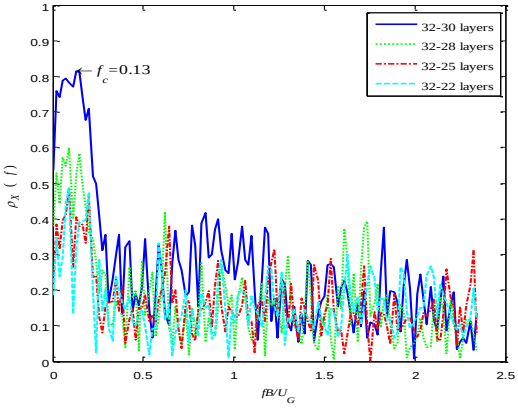

(b) middle-upper part
(measurement taps of group A)

Continued-

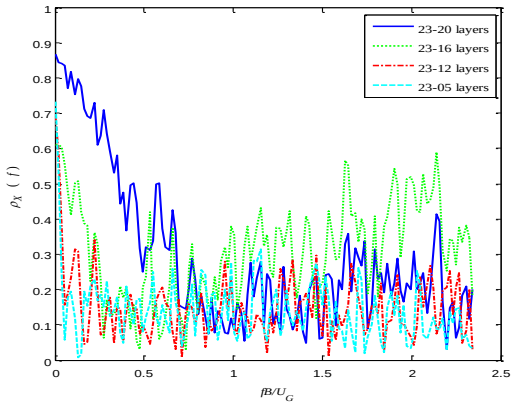

(c) middle-lower part
(measurement taps of group C)

Fig. 12 Coherence functions of wind force coefficients along X-axis (along-wind) in wind direction 45°

(Note: $f_c = fB/U_G$ is the reduced frequency; B is the characteristics width perpendicular to the Y-axis ; U_G is the gradient wind speed)

As shown in Fig.13, the coherence functions along the Y-axis (across-wind) have two peaks at the top and upper part of the main structure. As the height decreases, the distances of the two peaks decrease gradually and ultimately only one peak at the middle-lower part of the main structure remains as the width ratios of along-wind to across-wind increase. These features were akin to the across-wind force spectra for rectangular tall buildings with various side ratios, which are investigated in detail by Liang *et al*. (2002). As shown in Fig. 14, the coherence functions around the Z-axis (torsional-wind) are similar to that of the Y-axis (across-wind). Their features are something similar to the torque spectra of rectangular tall buildings with various side ratios, as investigated by Liang *et al*. (2004). Unfortunately, the researches by Liang *et al.* (2002, 2004) and other scholars mainly focused on the characteristics and mathematical expressions of wind force spectra but pay little attention to the coherence functions of wind forces, especially that of across-wind and torsional-wind.

4. Mathematical expressions for vertical coherence functions of wind forces

As mentioned, the shape of the building is symmetrical about the X- and Y-axes. Moreover, for the wind direction of 315°, the Y direction of body-axis expresses the along-wind of wind field axis, the X direction of body-axis expresses the across-wind of wind field axis, and the RZ direction of body-axis expresses the torsion-wind of wind field axis. Therefore, the mathematical expressions, as well as the inductive analysis method for summarizing fitted parameters of the coherence functions of wind forces, would focus on the wind direction of 315°.

4.1 X-axis direction (across-wind)

If the abscissae in Fig. 6 are changed to $f\Delta z/\bar{U}_z$, the peaks of the coherence functions would be staggered, as shown in Fig. 15, therefore, the coherence functions can not be fitted by the traditional exponential formula in the same coordinates like wind speeds but have to be fitted one by one using suitable formulae, and then the inductive analysis method are used to summarize the relations of the fitted parameters. With reference to the coherence functions of wind speeds, two types for formulae of coherence functions of across-wind forces would be proposed.

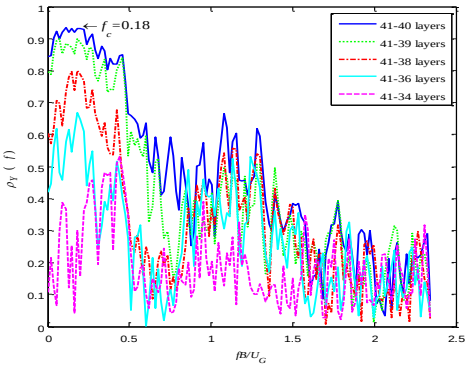

Continued-

(a) top
(measurement taps of group A)

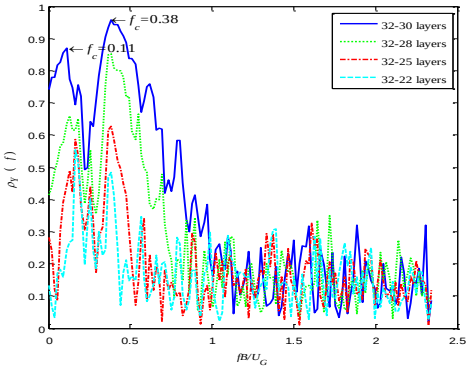

(b) middle-upper part
(measurement taps of group A)

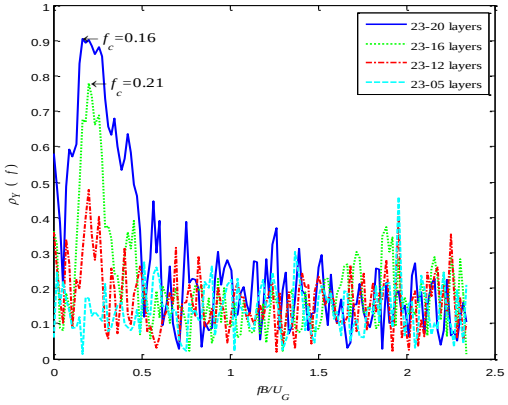

(c) middle-lower part
(measurement taps of group C)

Fig. 13 Coherence functions of wind force coefficients along Y-axis (across-wind) in wind direction 45°

(Note: $f_c = fB/U_G$ is the reduced frequency; B is the characteristics width perpendicular to the Y-axis; U_G is the gradient wind speed)

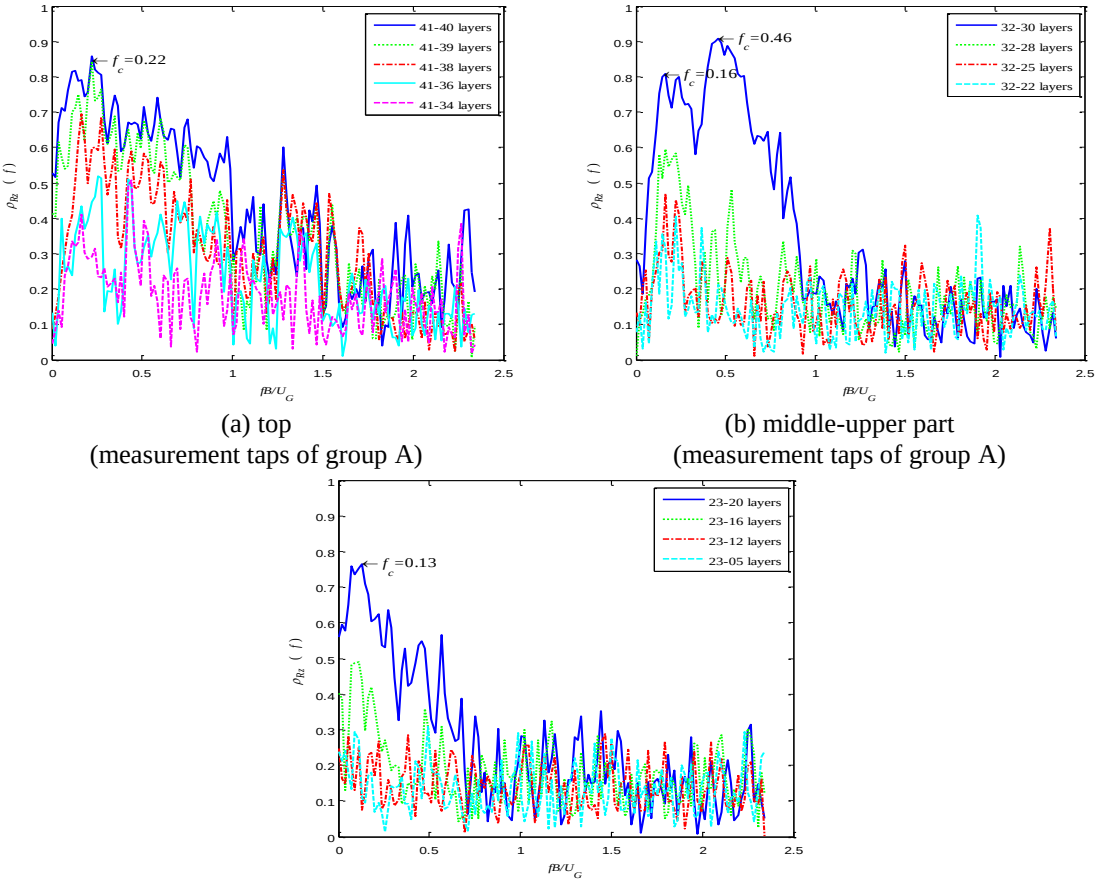

(a) top
(measurement taps of group A)

(b) middle-upper part
(measurement taps of group A)

(c) middle-lower part
(measurement taps of group C)

Fig. 14 Coherence functions of wind force coefficients around Z-axis (torsional-wind) in wind direction 45^o

(Note: $f_c = fB/U_G$ is the reduced frequency; B is the characteristics width perpendicular to the Y-axis; U_G is the gradient wind speed)

4.1.1 Formula I

It is well known that the mathematical expression of the coherence function of wind speeds proposed by Davenport (1965) is

$$\rho(f) = \exp(-C_1 f_c) \tag{4}$$

Where $f_c = f\Delta z/\overline{U}_z$ is the reduce frequency; f is the frequency; $\overline{U}_z$ is the average wind speed of the two points considered; Δz is the distance between the two points considered; C_1 is defined as the exponential decay coefficient.

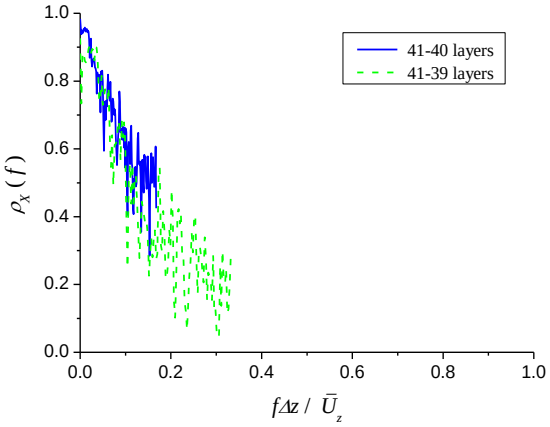

(a) top (group A)

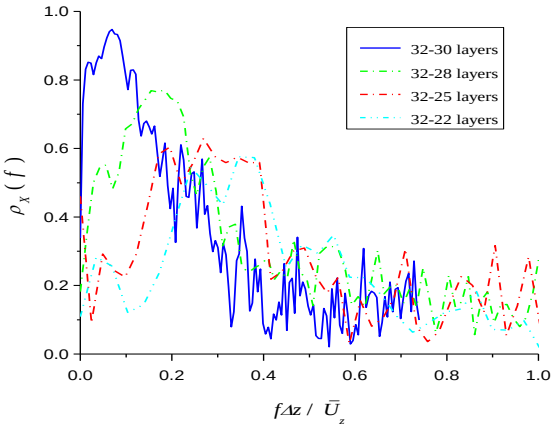

(b) middle-upper part (group A)

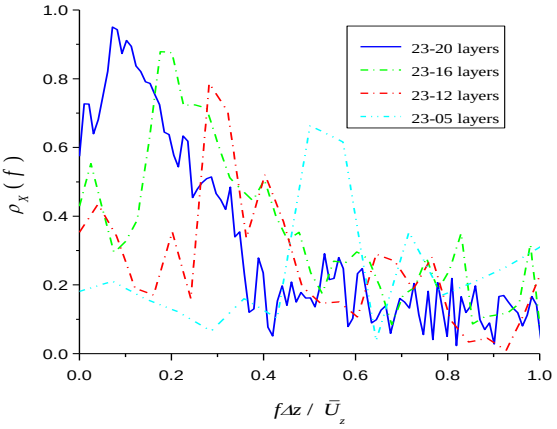

(c) middle-lower part (group C)

Fig. 15 Coherence functions of wind force coefficients along X-axis (across-wind) in wind direction 315°

Referencing Eq.(4), the coherence functions of X-axial (across-wind) wind forces at different levels of altitude can be fitted with the following formula superimposed by an exponential decay function and a peak function, which are respectively caused by turbulent flow and vortex shedding

$$\rho_X(f) = A_1 \exp(-C_1 f_c) + A_2 \exp\left[-(f_c - S_t \cdot \frac{\Delta z}{B} \cdot \frac{U_G}{\bar{U}_z})^2 \Big/ C_2^2\right] \tag{5}$$

Where $f_c = f\Delta z/\bar{U}_z$; S_t is the reduced frequency of vortex shedding; U_G is the gradient wind speed; $\bar{U}_z$ is the average wind speed of two measurement levels; B is the characteristic width; A_1, A_2, C_1, and C_2 are four parameters to be determined.

In Eq. (5), the first term is Eq. (4) multiplied by A_1, which is used to consider the "head drop" effects at low frequencies (i.e., the coherence function is less than 1 when the reduced frequency is equal to zero).

The coherence functions between two measurement levels, i.e., 41-40, 41-39, 32-30, 32-28, 32-25, 32-22, 23-20, 23-16, 23-12, 23-09, and 23-05, are curve-fitted using Eq. (5), and the corresponding fitting parameters are listed in Table 2. Fig. 16 shows the fitted results from measurement levels 32-30 and 23-20: the Eq. (5) matches the test data well.

Table 2 Fitting results of coherence functions of wind forces at typical levels along X-axis (across-wind) in wind direction 315°

Direction	Measurement level	Δz (m)	$\bar{U}_z$ (m/s)	$\bar{Z}$ (m)	S_t	A_1	A_2	C_1	C_2
X-axis	41-40	0.0150	9.0000	1.3904	0.23	0.9680	0.0500	4.4893	0.0070
	41-39	0.0300	9.0000	1.3829	0.23	0.9147	0.1089	5.3330	0.0186
	32-30	0.0660	8.9621	1.1878	0.23	0.8500	0.2700	3.0000	0.0360
	32-28	0.1597	8.8798	1.1409	0.23	0.5000	0.4100	1.8000	0.0840
	32-25	0.2735	8.7719	1.0840	0.21	0.3346	0.4300	0.9697	0.1100
	32-22	0.3815	8.6596	1.0300	0.17	0.2300	0.4400	0.4697	0.1200
	23-20	0.1080	8.2700	0.8213	0.19	0.7094	0.3600	2.0112	0.0590
	23-16	0.2589	8.0848	0.7459	0.16	0.4345	0.5030	0.9966	0.0850
	23-12	0.4037	7.8624	0.6734	0.15	0.3200	0.5400	0.9400	0.0880
	23-09	0.5151	7.6515	0.6178	0.15	0.1758	0.5600	0.2086	0.0890
	23-05	0.6634	7.2709	0.5436	0.14	0.1400	0.5700	0.1000	0.0900

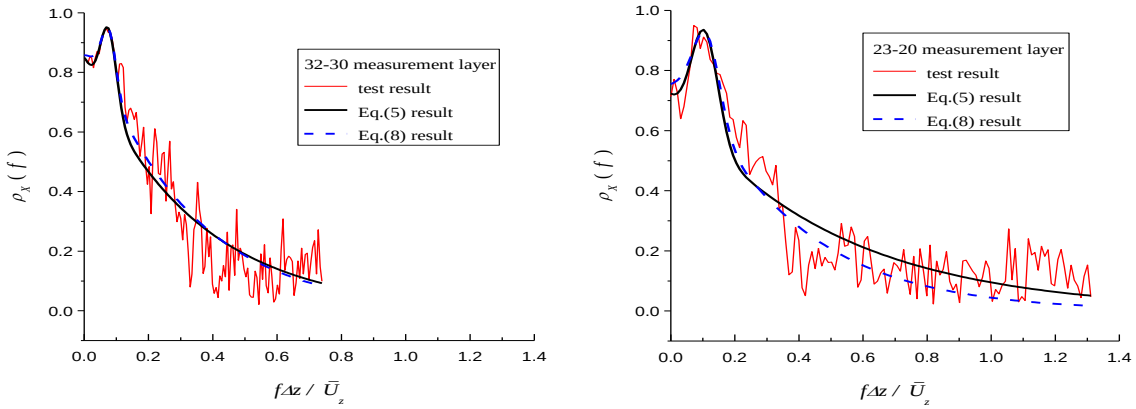

Fig. 16 Fitting results of coherence functions of wind forcesat typical levels along X-axis (across-wind) in wind direction 315°

(Note: $f_c = \Delta Z / \bar{U}_z$ is the reduced frequency; $\bar{U}_z$ is the average wind speed of the two points considered, Δz is the distance between the two points considered)

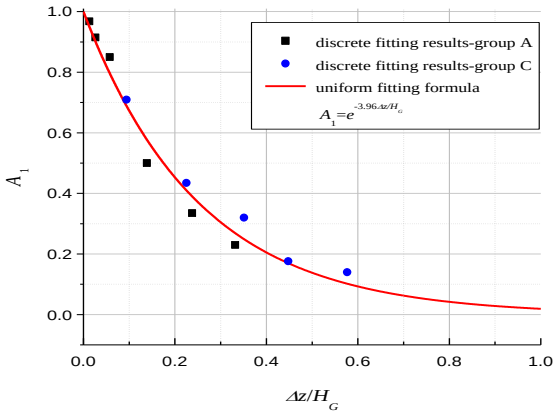

(a) parameterA_1

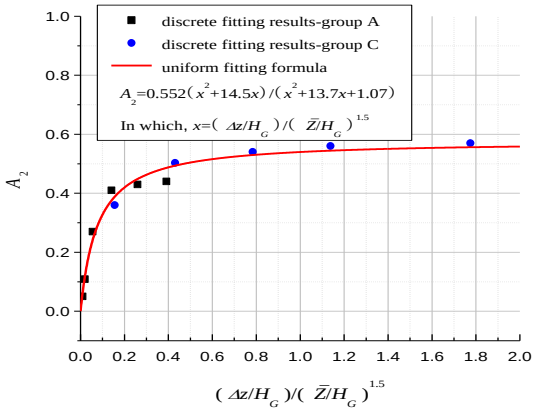

(b) parameter A_2

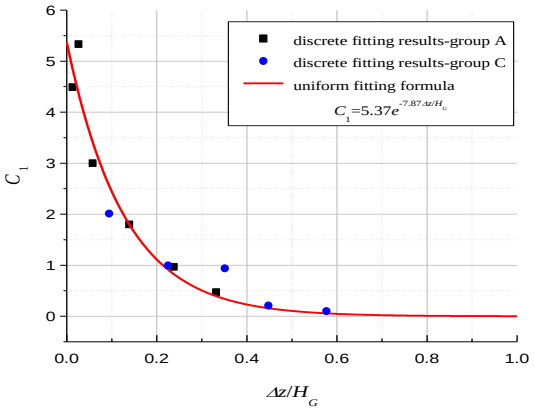

(c) parameter C_1

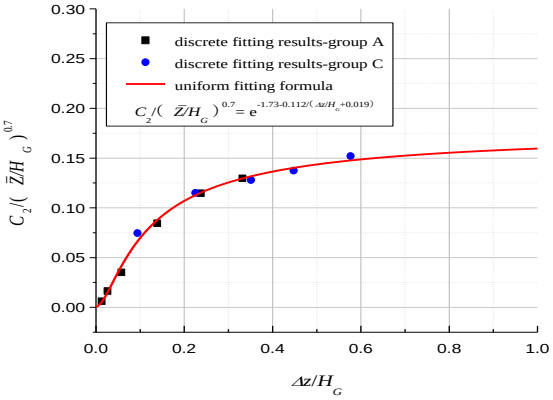

(d) parameter C_2

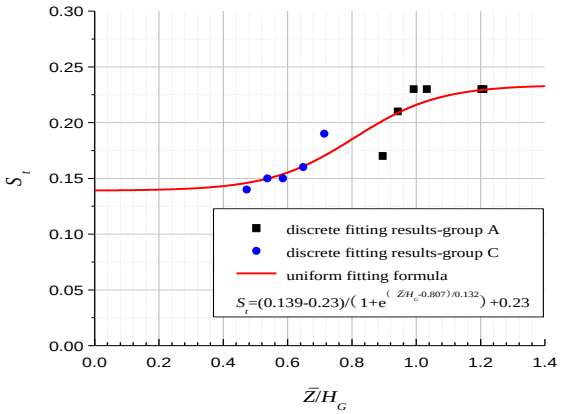

(e) parameter S_t

Fig. 17 Parametric fitted results for coherence functions of wind forces along X-axis (across-wind) in wind direction 315°

The fitting results of parameters A_1, A_2, C_1, C_2, and S_t (see Table 2) can be put into five unified coordinates, as shown in Fig. 17, and then fitted by the following formulae

$$A_1 = e^{-3.96\Delta z / H_G} \tag{6a}$$

$$A_2 = 0.552(x^2+14.5x)/(x^2+13.7x+1.07) \tag{6b}$$

$$C_1 = 5.37e^{-7.87\Delta z / H_G} \tag{6c}$$

$$C_2 = \mathrm{e}^{-1.73-0.112/(\Delta z / H_G+0.019)}(\bar{Z}/H_G)^{0.7} \tag{6d}$$

$$S_t = \frac{0.139-0.23}{1+e^{(\bar{Z}/H_G-0.807)/0.132}}+0.23 \tag{6e}$$

In which $x=(\Delta z / H_G)/(\bar{Z}/H_G)^{1.5}$; H_G is the gradient height; $\bar{Z}$ is the mean height of the two positions considered.

For the opening at the top, the above formulae are also applicable.

Figs. 17(b) and 17(d) show that the parameters A_2 and C_2 are related not only to the distance between two levels of wind forces but also to their average height, therefore, Fig. 18 gives their relationship with three-dimensional surfaces.

4.1.2 Formula II

A modified exponential decay function for the coherence function of wind speeds, which was well coincide with the measured results of "head drop" at low frequencies(i.e., the coherence function is less than 1 when the reduced frequency is equal to zero.), was derived by Krenk (1995), Hansen and Krenk (1999).

$$\rho(f) = (1-\frac{1}{2}C_1 f_c^*)\exp(-C_1 f_c^*) \tag{7a}$$

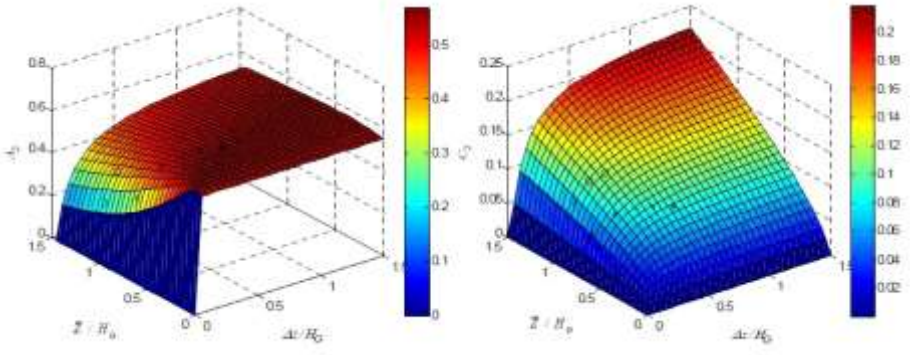

(a) A_2 (b) C_2

Fig. 18 Relationship curves for parameters A_2 and C_2

$$f_c^* = \frac{\Delta z}{\bar{U}_z}\sqrt{f^2 + \frac{1}{70.78}\left(\frac{\bar{U}_z}{L_a^x}\right)^2} \tag{7b}$$

Where C_1 is the exponential decay coefficient; L_a^x is the turbulent flow integral length scale. with reference to Eq. (7), another modified exponential decay function can be used to substitute the first term of Eq. (5), therefore, the coherence function of wind force along X axis (across-wind) can be rewritten as

$$\rho_X(f) = \exp(-C_1 f_c^*) + A_2 \exp\left[-(f_c - S_t \cdot \frac{\Delta z}{B} \cdot \frac{U_G}{\bar{U}_z})^2 \Big/ C_2^2\right] \tag{8}$$

where $f_c = f\Delta z/\bar{U}_z$; $f_c^* = \frac{\Delta z}{\bar{U}_z}\sqrt{f^2 + A_1^2}$; S_t is the reduced frequency of vortex shedding; U_G is the gradient wind speed; $\bar{U}_z$ is the mean wind speed between two measurement levels of altitude; B is the characteristic width; A_1, A_2, C_1, and C_2 are parameters to be determined.

The coherence functions between two measurement levels of altitude, i.e., 41-40, 41-39, 32-30, 32-28, 32-25, 32-22, 23-20, 23-16, 23-12, 23-09, and 23-05, are fitted using Eq. (8), and the corresponding fitting parameters are listed in Table 3. In addition, the fitted results by Eq. (8) at measurement levels of 32-30 and 23-20 (see Fig. 21) show that it is also an ideal formula for the coherence functions of X-axial (across-wind) wind forces at different levels of altitude.

Table 3 Fitting results of modified coherence function of wind forces at typical levels along X-axis (across-wind) in wind direction 315°

Direction	Measurement level	Δz (m)	$\bar{U}_z$ (m/s)	$\bar{Z}$ (m)	S_t	A_1	A_2	C_1	C_2
X-axis	41-40	0.0150	9.0000	1.3904	0.19	12.096	0.0633	4.7031	0.0099
	41-39	0.0300	9.0000	1.3829	0.19	8.309	0.0921	5.790	0.0198
	32-30	0.0660	8.9621	1.1878	0.23	5. 242	0.2180	3.3598	0.0290
	32-28	0.1597	8.8798	1.1409	0.23	15.963	0.3407	2.4335	0.0840
	32-25	0.2735	8.7719	1.0840	0.21	25.382	0.3984	1.6115	0.1100
	32-22	0.3815	8.6596	1.0300	0.17	32.715	0.4294	1.2033	0.1200
	23-20	0.1080	8.2700	0.8213	0.20	7.2144	0.2880	3.101	0.0590
	23-16	0.2589	8.0848	0.7459	0.17	15.10	0.4133	1.6497	0.0850
	23-12	0.4037	7.8624	0.6734	0.155	23.4658	0.4499	1.1765	0.0880
	23-09	0.5151	7.6515	0.6178	0.15	30.6151	0.4761	0.735	0.0890
	23-05	0.6634	7.2709	0.5436	0.14	35.8749	0.5223	0.523	0.0900

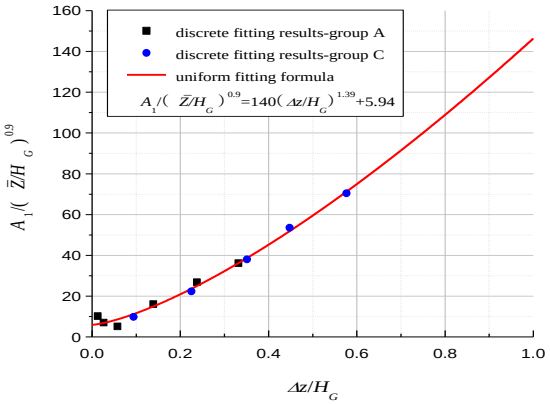

(a) parameterA_1

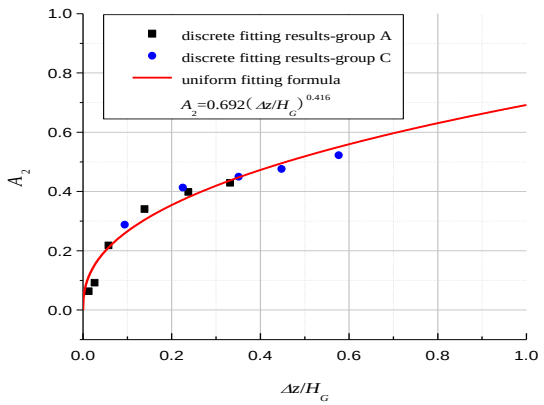

(b) parameter A_2

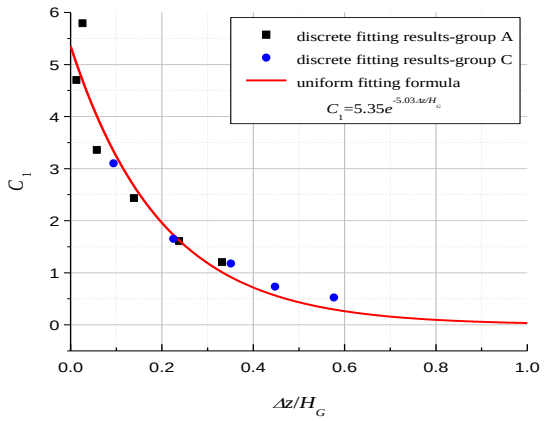

(c) parameter C_1

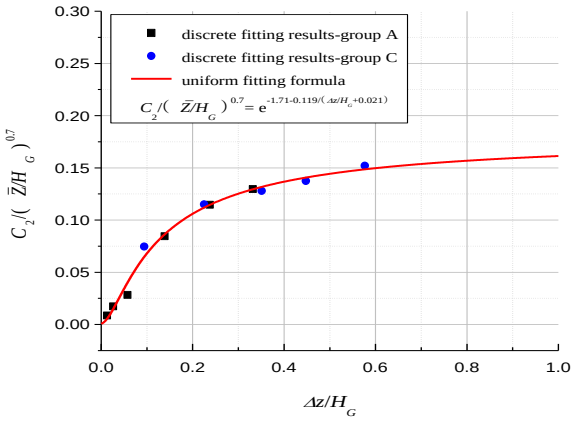

(d) parameter C_2

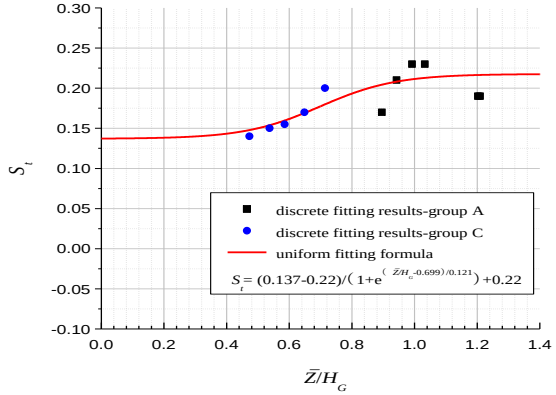

(e) parameter S_t

Fig. 19 Parametric fitted results for modified coherence functions of wind forces along X-axis (across-wind) in wind direction 315°

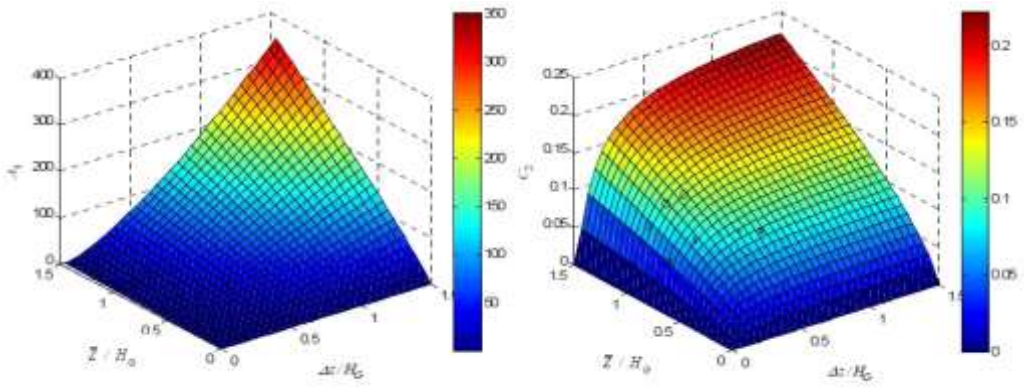

(a) A_2 (b) C_2

Fig. 20 Relationship curves for parameters A_2 and C_2

The fitting parameters of each coherence function (see Table 3) can be put into unified coordinates respectively, as shown in Fig. 19, and then be fitted by the following formulae

$$A_1 = \left[140(\Delta z / H_G)^{1.39} + 5.94\right] \cdot \left(\bar{Z}/H_G\right)^{0.9} \tag{9a}$$

$$A_2 = 0.692(\Delta z / H_G)^{0.416} \tag{9b}$$

$$C_1 = 5.35e^{-5.03\Delta z / H_G} \tag{9c}$$

$$C_2 = \mathrm{e}^{-1.71-0.119/(\Delta z / H_G + 0.021)} \cdot (\bar{Z} / H_G)^{0.7} \tag{9d}$$

$$S_t = \frac{0.137 - 0.22}{1 + e^{(\bar{Z}/H_G - 0.699)/0.121}} + 0.22 \tag{9e}$$

Figs. 19(b) and 19(d) show that the parameters A_2 and C_2 are related not only to the distance of the wind forces at two levels of altitude but also to their average height, therefore, Fig. 20 gives their relationship with three-dimensional surfaces.

4.2 Y axis direction (along-wind)

As shown in Fig. 7, the coherence functions of wind forces along the Y-axis (along-wind) have no peaks of vortex shedding, therefore, they can be fitted by two methods: one is called the comprehensive analysis method, i.e., all the coherence functions are fitted in the same coordinates akin to the traditional exponential format used for wind speeds; another is the afore mentioned inductive analysis method, i.e., the coherence functions are fitted one by one using suitable formulae and then the relations of the fitted parameters are summarized. However, the former cannot consider the “head drop” effects at low frequencies, unlike the latter.

4.2.1 Formula I

If the abscissae in Fig. 7 are changed to $f\Delta z/\bar{U}_z$, the test data for the coherence functions can be fitted in the same coordinates as the wind speeds except at low frequencies. The fitted formula for the coherence functions of the wind forces along the Y-axis (along-wind), akin to that of the wind speeds (Eq. (4)), can be expressed as

$$\rho_Y(f)=\exp(-C_1 f_c) \tag{10}$$

where $f_c = f\Delta z/\bar{U}_z$; C_1 is the exponential decay coefficient to be determined.

The coherence functions between two measurement levels, *i.e.*41-40, 41-39, 41-30, 41-28, 41-25, 41-22, 32-30, 32-28, 32-25, 32-22, 27-26, 27-24, 27-21, 27-19, 27-17, 27-15, 23-20, 23-16, 23-12, 23-09, and 23-05, are put into the same coordinates and fitted by Eq. (10) (some data at low frequencies were ignored), as shown in Fig. 21. The fitted exponential decay coefficients

$$C_1 = 6.0 \tag{11}$$

This is smaller than the exponential decay coefficient of along-wind (10.2) and larger than that of across-wind (4.34), which was discussed by Huang *et al*. (2009).

4.2.2 Formula II

To improve the fitting effects at low frequencies, amodified exponential formula for coherence functions of wind forces at different levels of altitude along the Y-axis (along-wind) is proposed as follows

$$\rho_Y(f)=A_1\exp(-C_1 f_c) \tag{12}$$

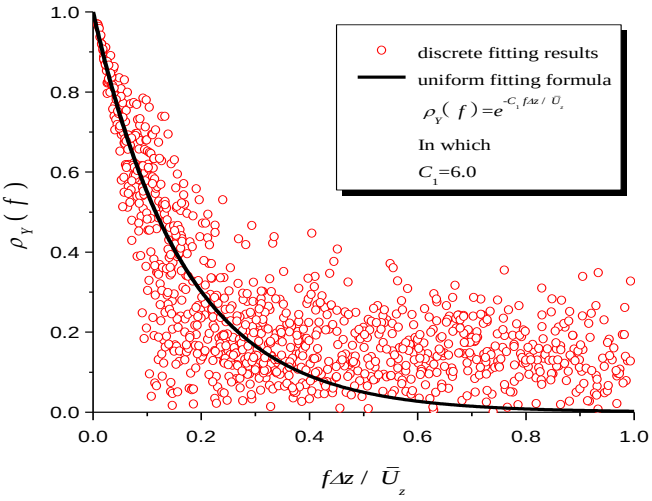

Fig. 21 Fitting results for coherence functions of wind forces along Y-axis (along-wind) in wind direction 315°

Where $f_c = f\Delta z/\bar{U}_z$; A_1 and C_1 are parameters to be determined.

The coherence functions between two measurement levels of altitude, i.e., 41-40, 41-39, 32-30, 32-28, 32-25, 32-22, 23-20, 23-16, 23-12, 23-09, and 23-05, are fitted using Eq. (12) respectively, and the corresponding fitting parameters are listed in Table 4. Furthermore, the fitted data at measurement levels of 32-30 and 23-20 are given in Fig. 22, which shows that Eq. (12) is an ideal formula for the coherence functions of wind forces at different levels of altitude in the Y-axis direction (along-wind).

Table 4 Fitting results of coherence function of wind forces at typical levels along Y-axis (along-wind) in wind direction 315°

Direction	Measurement level	Δz (m)	$\bar{U}_z$ (m/s)	$\bar{Z}$ (m)	A_1	C_1
Y-axis	41-40	0.0150	9.0000	1.3904	0.991	5.270
	41-39	0.0300	9.0000	1.3829	0.9834	7.6237
	32-30	0.0660	8.9621	1.1878	0.970	3.859
	32-28	0.1597	8.8798	1.1409	0.822	3.545
	32-25	0.2735	8.7719	1.0840	0.712	3.3143
	32-22	0.3815	8.6596	1.0300	0.628	3.0763
	23-20	0.1080	8.2700	0.8213	0.7919	3.7992
	23-16	0.2589	8.0848	0.7459	0.5930	3.3477
	23-12	0.4037	7.8624	0.6734	0.465	2.9830
	23-09	0.5151	7.6515	0.6178	0.411	2.427
	23-05	0.6634	7.2709	0.5436	0.3364	1.927

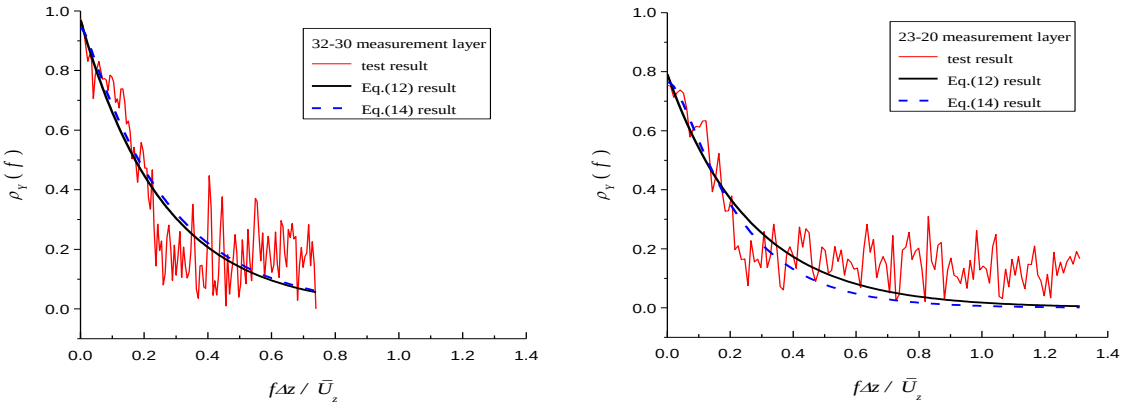

Fig. 22 Fitting results for coherence functions of wind forces at typical levels along Y-axis (along-wind) in wind direction 315°

The fitting results of parameters A_1 and C_1 are put into two unified coordinates, respectively, as shown in Fig. 23, and then the following formulae are used to fit them

$$A_1 = \left\{1.0 + 27.4\left[(\Delta z / H_G)/(\bar{Z} / H_G)^{1.5}\right]^{1.64}\right\}^{-0.253} \tag{13a}$$

$$C_1 = 4.22\mathrm{e}^{-1.22(\Delta z / H_G)} + 3.57\mathrm{e}^{-33.9(\Delta z / H_G)} \tag{13b}$$

Fig. 23(a) shows that the parameter A_1 is related, not only to the distance of wind forces between two levels of altitude, but also to their average height, therefore, their relationship is a three-dimensional surface, see Fig. 24.

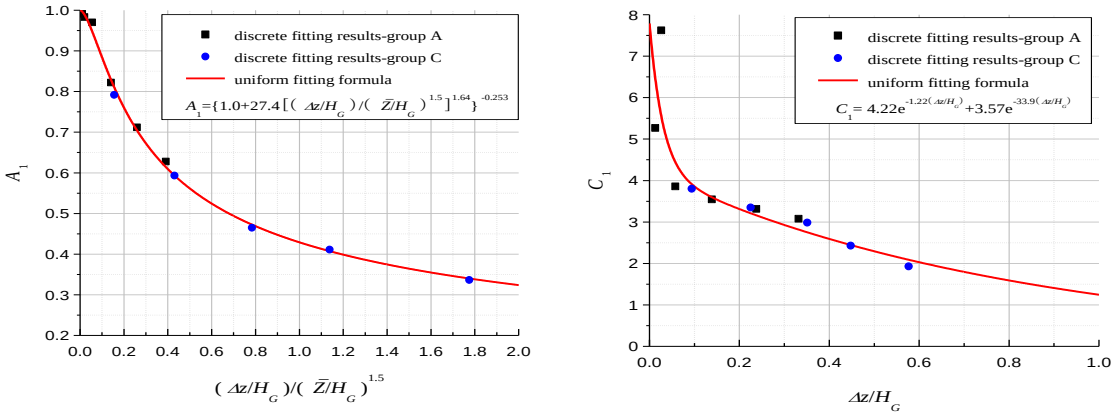

(a) parameter A_1 (b) parameter A_2

Fig. 23 Parametric fitted results for modified coherence functions of wind forces along Y-axis (along-wind) in wind direction 315°

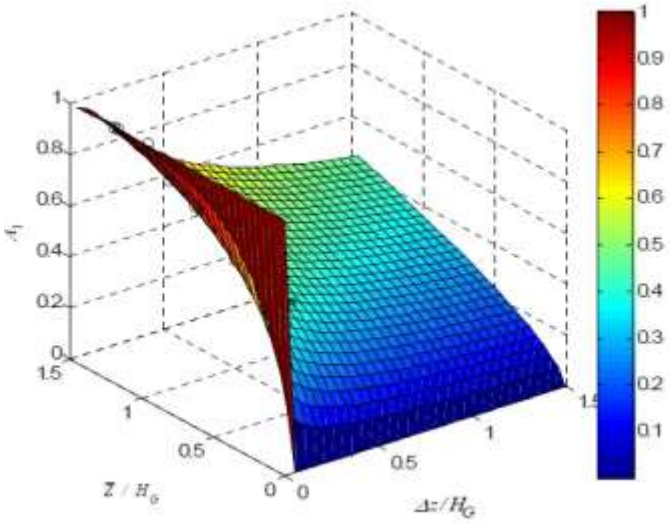

Fig. 24 Relationship curve for parameter A_1

Referring to Eq. (7), another modified exponential decay function can be used to substitute Eq. (12) for the coherence function of the wind force along the Y-axis (across-wind):

$$\rho_Y(f) = \exp(-C_1 f_c^*) \tag{14}$$

where $f_c^* = \frac{\Delta z}{\bar{U}_z}\sqrt{f^2 + A_1^2}$; A_1 and C_1 are parameters to be determined.

The fitted results at measurement levels of 32-30 and 23-20, using Eq. (14) (see Fig. 22), are satisfactory. The fitted results at other measurement levels are not discussed in detail here.

4.3 RZ-axis direction (torsional-wind)

It can be seen from Figs. 6 and 8 that the features of coherence functions around the Z-axis (torsional-wind) are similar to that of the X-axis (across-wind), therefore, their mathematical formula can also be expressed in the following format

$$\rho_{RZ}(f) = A_1 \exp(-C_1 f_c) + A_2 \exp\left[-(f_c - S_t \cdot \frac{\Delta z}{B} \cdot \frac{U_G}{\bar{U}_z})^2 \Big/ C_2^2\right] \tag{15}$$

Where $f_c = f\Delta z/\bar{U}_z$; S_t is the reduced frequency of vortex shedding; U_G is the gradient wind speed; $\bar{U}_z$ is the average wind speed between two measuring levels of altitude; B is the characteristic width; A_1, A_2, C_1, and C_2 are four fitting parameters.

The coherence functions between two measurement levels of altitude, i.e., 41-40, 41-39, 32-30, 32-28, 32-25, 32-22, 23-20, 23-16, 23-12, 23-09, and 23-05, are fitted using Eq. (15), and the corresponding fitting parameters are listed in Table 5.

The fitting results of parameters A_1, A_2, C_1, C_2, and S_t are put into five unified coordinates, respectively, as shown in Fig. 25, and the following formulae are then used to fit them

$$A_1 = e^{-5.19\Delta z/H_G} \tag{16a}$$

$$A_2 = 0.589(x^2 + 0.234x)/(x^2 + 0.783x + 0.00905) \tag{16b}$$

$$C_1 = 5.53e^{-8.94\Delta z/H_G} \tag{16c}$$

$$C_2 = \mathrm{e}^{-2.19-0.0789/(\Delta z/H_G + 0.00989)}(\bar{Z}/H_G)^2 \tag{16d}$$

$$S_t = 0.162 \tag{16e}$$

In which $x = (\Delta z/H_G)/(\bar{Z}/H_G)^5$

Figs. 25(b) and 25(d) show that parameters A_2 and C_2 are related not only to the distance of the wind forces between two levels of altitude but also to their average height, therefore, their relationshipcan be shown with three-dimensional surfaces (see Fig. 26).

To confirm the effectiveness of the proposed mathematical expressions for the coherence functions of wind loads, comparison of their generalized force spectra with test results is under taken.

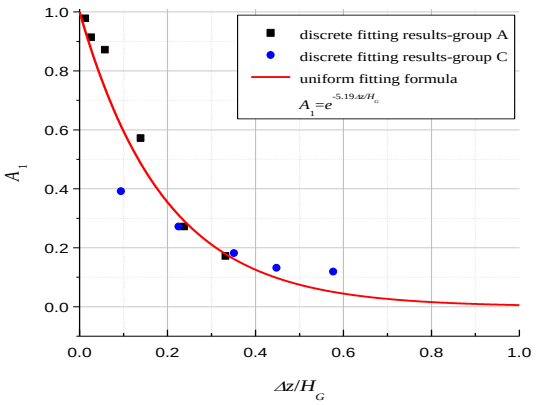

(a) parameterA_1

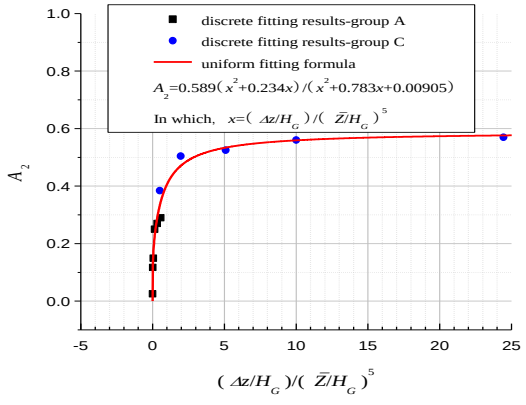

(b) parameter A_2

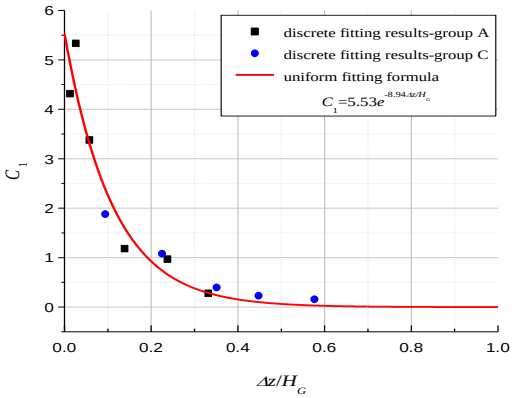

(c) parameter C_1

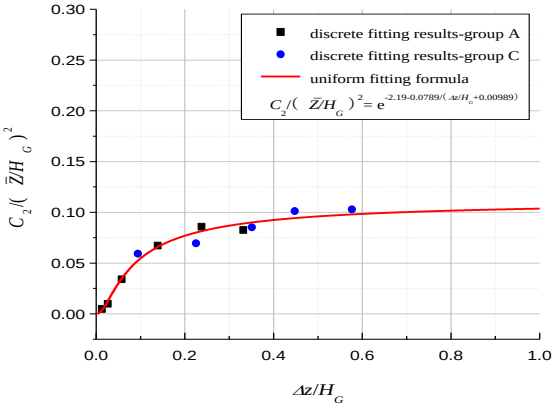

(d) parameter C_2

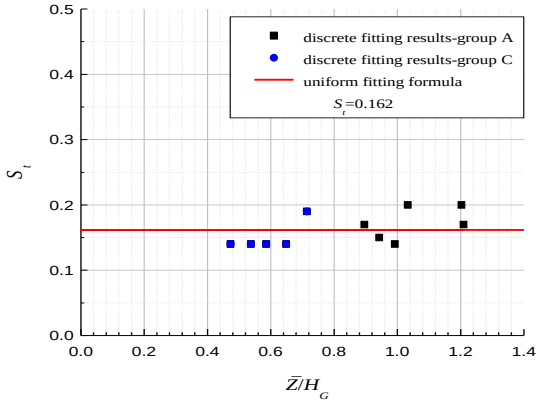

(e) parameter S_t

Fig. 25 Parametric fitted results for coherence functions of wind forces around Z-axis (torsional-wind) in wind direction 315^o

Table 5 Fitting results of coherence function of wind forces at typical levels around Z -xis (torsional-wind) in wind direction 315°

Direction	Measurement level	Δz (m)	$\bar{U}_z$ (m/s)	$\bar{Z}$ (m)	S_t	A_1	A_2	C_1	C_2
RZ-axis	41-40	0.0150	9.0000	1.3904	0.17	0.9781	0.025	4.3170	0.0070
	41-39	0.0300	9.0000	1.3829	0.20	0.9141	0.1169	5.3303	0.0142
	32-30	0.0660	8.9621	1.1878	0.20	0.8719	0.1492	3.3795	0.0362
	32-28	0.1597	8.8798	1.1409	0.14	0.5719	0.2500	1.1795	0.0662
	32-25	0.2735	8.7719	1.0840	0.15	0.2719	0.2700	0.9697	0.0762
	32-22	0.3815	8.6596	1.0300	0.17	0.1719	0.2900	0.2795	0.0662
	23-20	0.1080	8.2700	0.8213	0.19	0.3919	0.3840	1.8795	0.0302
	23-16	0.2589	8.0848	0.7459	0.14	0.2719	0.5040	1.0795	0.0292
	23-12	0.4037	7.8624	0.6734	0.14	0.1819	0.5250	0.3950	0.0292
	23-09	0.5151	7.6515	0.6178	0.14	0.1319	0.5600	0.2270	0.0292
	23-05	0.6634	7.2709	0.5436	0.14	0.1190	0.5700	0.1570	0.0230

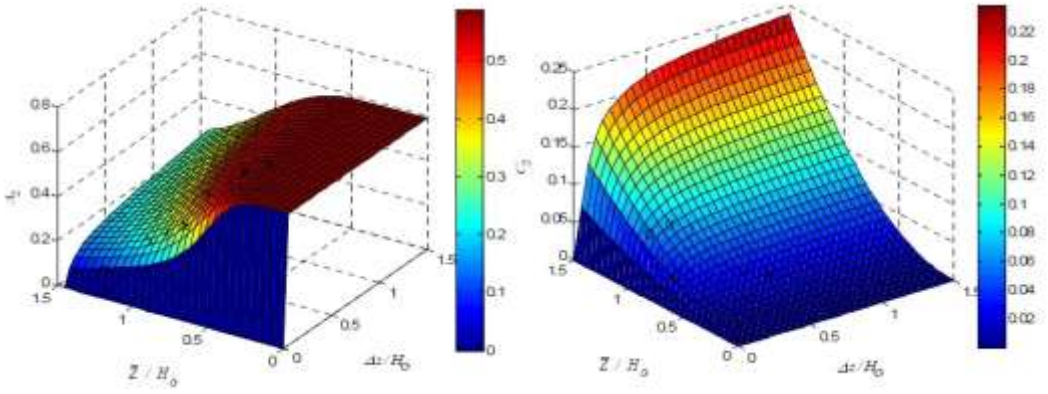

(a) A_2 (b) C_2

Fig. 26 Relationship curves for parameters A_2 and C_2

5. Effectiveness of mathematical expressions of coherence functions by comparison of generalized force spectra

To confirm the effectiveness of the proposed mathematical expressions for the coherence functions of wind loads, comparison of their generalized force spectra with test results is undertaken.

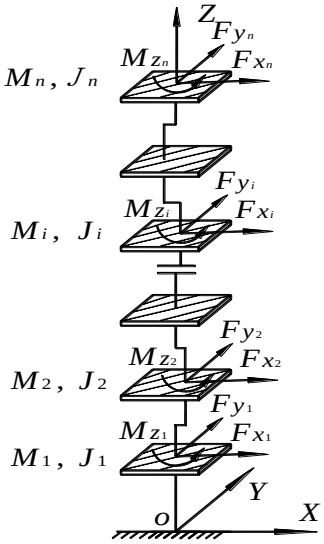

Fig. 27 Rigid-floor model

If the dynamic finite element method (FEM) model of tall building is simplified as a series rigid-floor model by selecting the centroid of each rigid-floor as the coordinate origin, as shown in Fig. 27, a *n*-floors tall building will have *n* rigid-floor masses, each with two translational degrees of freedom and one rotational degree of freedom, that is, 3*n* degrees of freedom in all. Therefore, the equation of motion can be expressed as

$$\boldsymbol{M}\ddot{\delta}(t)+\boldsymbol{C}\dot{\delta}(t)+\boldsymbol{K}\delta(t)=\boldsymbol{R}F(t) \tag{17}$$

where, $\boldsymbol{M}$, $\boldsymbol{C}$ and $\boldsymbol{K}$ are the $3n\times3n$ mass, damping, and stiffness matrices, respectively; $\boldsymbol{\delta}$ is the $3n$-dimensional displacement vector; $F(t)$ is the $3m$-dimensional vector of random fluctuating wind loads on the measurement levels of altitude with zero mean value; $\boldsymbol{R}$ is a $3n\times3m$ deterministic matrix for transforming the wind loads on pressure measurement levels of altitude to those on the actual building's floors, and *m* is the number of measurement levels of altitude.

$$\delta(t)=\begin{Bmatrix}\{x(t)\}\\ \{y(t)\}\\ \{\theta(t)\}\end{Bmatrix}=\{x_1(t),\cdots,x_i(t),\cdots,x_n(t),y_1(t),\cdots,y_i(t),\cdots,y_n(t),\theta_1(t),\cdots,\theta_i(t),\cdots,\theta_n(t)\}^{\mathrm{T}}$$

$$\boldsymbol{M}=\begin{bmatrix}\boldsymbol{M}_{xx} & & 0\\ & \boldsymbol{M}_{yy} & \\ 0 & & \boldsymbol{J}_{\theta\theta}\end{bmatrix},\quad \boldsymbol{M}_{xx}=\boldsymbol{M}_{yy}=\begin{bmatrix}M_1 & & & 0\\ & M_2 & & \\ & & \ddots & \\ 0 & & & M_n\end{bmatrix},$$

$$\boldsymbol{J}_{\theta\theta}=\begin{bmatrix} J_1 & & & 0 \\ & J_2 & & \\ & & \ddots & \\ 0 & & & J_n \end{bmatrix},$$

$$\boldsymbol{F}(t)=\begin{Bmatrix} \boldsymbol{F}_x(t) \\ \boldsymbol{F}_y(t) \\ \boldsymbol{T}_z(t) \end{Bmatrix}=\left\{F_{x1}(t),\cdots,F_{xj}(t),\cdots,F_{xm}(t),F_{y1}(t),\cdots,F_{yj}(t),\cdots,F_{ym}(t),T_{z1}(t),\cdots,T_{zj}(t),\cdots,T_{zm}(t)\right\}^{\mathrm{T}} \quad (18)$$

where, $x_i(t)$, $y_i(t)$, and $\theta_i(t)$ are the displacement time histories of the i^{th} rigid-floor mass along X- and Y- axes, and round the Z-axis, respectively;
M_i and J_i are the mass and moment of inertia of i^{th} structural floor, respectively;
$F_{xj}(t)$, $F_{yj}(t)$, and $T_{zj}(t)$ are the wind force time histories of the j^{th} measurement level of altitude along the X-and Y- axes, and round the Z axis, respectively.

Eq. (17) can be decomposed by real modes when the aerodynamic damping, caused by air-structure interaction, is ignored. Let

$$\boldsymbol{\delta}(t)=\boldsymbol{\Phi}\boldsymbol{q}(t)=\sum_{j=1}^{3n}\varphi_j q_j(\mathrm{t}) \quad (19)$$

where, $\boldsymbol{\varphi}_j$ is defined as the j^{th} structural mode; $q_j(\mathrm{t})$ is known as the j^{th} structural principal coordinates.

Substitute Eq. (19) into Eq. (17) and multiply by $\boldsymbol{\varphi}_j$ on both sides of the equation, the physical equation can be decoupled as the structural principal coordinates equation

$$\ddot{q}_j(t)+2\xi_j\omega_j\dot{q}_j(t)+\omega_j^2 q_j(t)=\bar{F}_j(t) \qquad (j=1,\cdots,3n) \quad (20)$$

where $\bar{F}_j(t)$ is the j^{th} generalized wind load which can be calculated as follows

$$\bar{F}_j(t)=\boldsymbol{\varphi}_j^{\mathrm{T}}\boldsymbol{R}F(t)\big/M_j^* \quad (21)$$

So the power spectrum function of $\bar{F}_j(t)$ is

$$S_{\bar{F}_j\bar{F}_j}(f)=\boldsymbol{\varphi}_j^{\mathrm{T}}\boldsymbol{R}\boldsymbol{S}_{FF}(f)\boldsymbol{R}^{\mathrm{T}}\boldsymbol{\varphi}_j\Big/\left(M_j^*\right)^2 \quad (22)$$

where $S_{\bar{F}_j\bar{F}_j}(f)$ denotes the j^{th} generalized force spectrum; $\boldsymbol{S}_{FF}(f)$ is a matrix constructed by the power spectra and coherence functions of the wind forces, however, $S_{\bar{F}_j\bar{F}_j}(f)$ is a single, comprehensive parameter in the frequency domain, therefore, comparison of $S_{\bar{F}_j\bar{F}_j}(f)$ is more simple and inductive than $\boldsymbol{S}_{FF}(f)$.

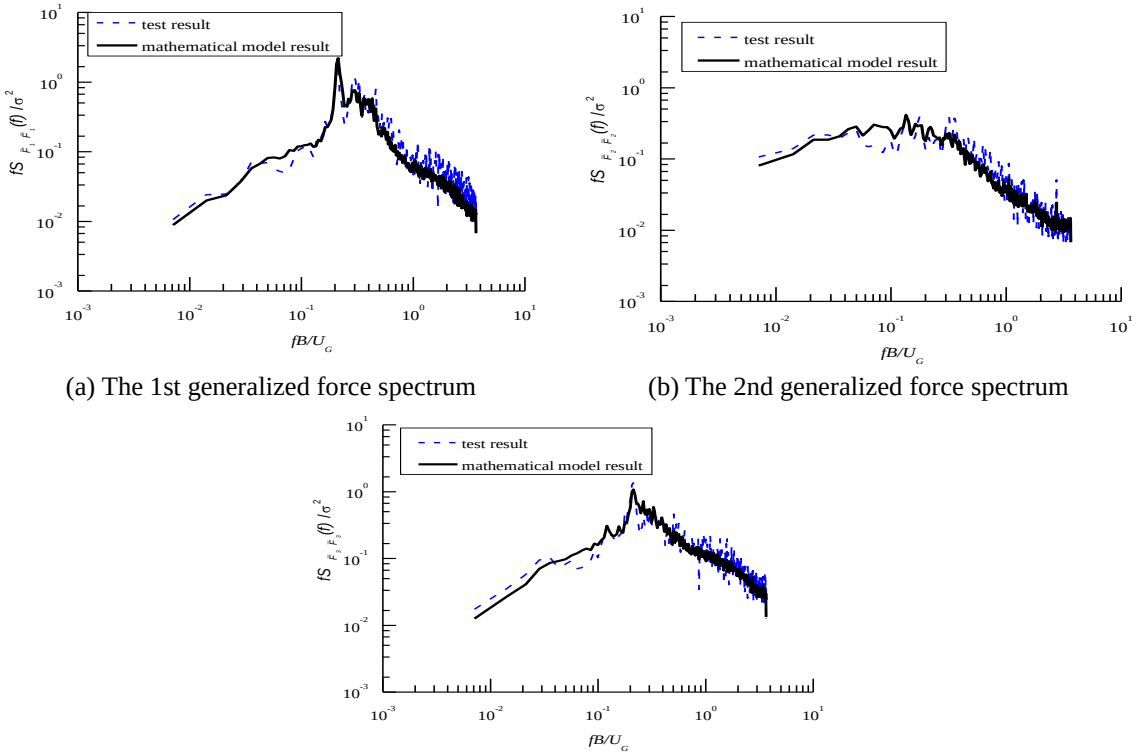

(a) The 1st generalized force spectrum (b) The 2nd generalized force spectrum

(c) The 3rd generalized force spectrum

Fig. 28 Comparisons of the generalized force spectra from the preceding three orders: mathematical model *versus* rigid model synchronization pressure test

There are two ways to obtain the power spectrum matrix $\boldsymbol{S}_{FF}(f)$: half-formula results or experimental results. The half-formula results relies on matrix diagonal elements, i.e., auto-power spectra, are obtained from a rigid model synchronization pressure experiment, and matrix non-diagonal elements, i.e., cross-power spectra are calculated according to Eq. (3), in which the auto-power spectra are acquired experimentally yet the coherence functions are obtained from the proposed mathematical expressions. The experimental results are such that not only the diagonal elements, but also the non-diagonal elements, are all acquired experimentally. It must be emphasized that the wind loads calculated by above two ways are only divided into two groups (A and C) in which correlation should be ignored for asynchrony, noting the corresponding change of A_{ij} and h_i in Eq. (2).

To verify the validity of the mathematical expressions of the coherence functions (Eqs. (5) and (6), Eqs. (12) and (13), and Eqs. (15) and (16)) proposed here, the first three orders' generalized force spectra (the first three order modes are shown in Fig. 5) obtained according to half-formula results are compared to those obtained by experiment results, as shown in Fig. 28: the comparisons showed good agreement.

6. Analysis of wind-induced dynamic responses based on mathematical expressions of wind forces

6.1 Influence of coherence functions on wind-induced dynamic responses

According to random vibration theory, the solution of Eq. (17) in the frequency-domain can be expressed as

$$\mathbf{S}_{\delta\delta}(f)=\mathbf{\Phi H}^{*}(f)\mathbf{\Phi}^{\mathrm{T}}\mathbf{R}\mathbf{S}_{\mathbf{FF}}(f)\mathbf{R}^{\mathrm{T}}\mathbf{\Phi H}^{\mathrm{T}}(f)\mathbf{\Phi}^{\mathrm{T}} \tag{23}$$

where, $\mathbf{H}(f)=\mathrm{diag}\left\{H_1(f),\cdots,H_j(f),\cdots,H_{3n}(f)\right\}$ is the $3n\times 3n$matrix of the generalized frequency response function, $\mathbf{H}^{*}(f)$ is the complex conjugate of $\mathbf{H}(f)$, and $H_j(f)$ is the j^{th} frequency response function, determined by

$$H_j(f)=\frac{1}{(2\pi f_j)^2-(2\pi f)^2+2i\xi_j(2\pi f)(2\pi f_j)} \tag{24}$$

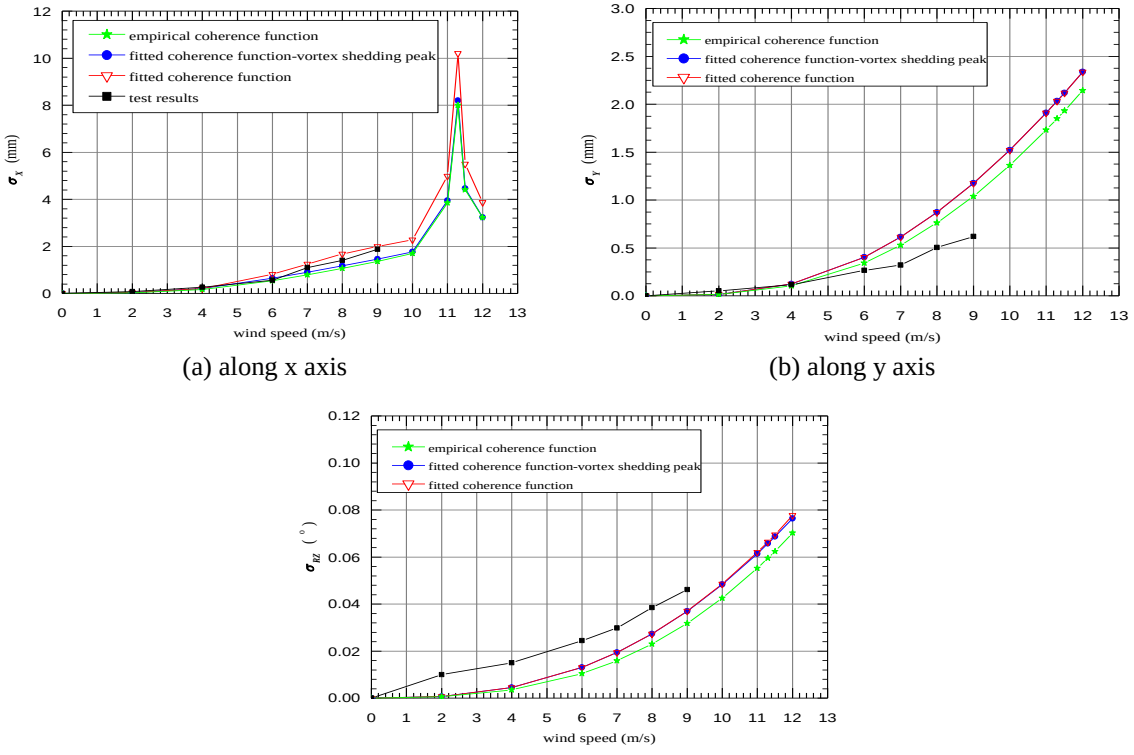

(a) along x axis

(b) along y axis

(c) around z axis

Fig. 29 Root of variances of displacement responses at top of building inwind direction 315°

The fundamental natural frequencies, modal damping ratios, and mode followed the aeroelastic model are listed in Table 1 and shown in Fig. 5.

As we all know, the wind speed at which vortex-induced resonance arose is

$$V_{cr}=\frac{fB}{S_t} \tag{25}$$

V_{cr} for this high-rise building is about 11.294 m/s when S_t is close to 0.137, as shown in Fig. 6. Therefore, the wind speed range for calculating the dynamic responses is 0 to 12 m/s.

Fig. 29 shows the root of the variances of the displacement response at the top of building for 315° wind direction based on the frequency domain method and the proposed mathematical expressions of wind loads (including power spectra and coherence functions). In the figures, the 'empirical coherence function' means that the power spectra matrix $\boldsymbol{S}_{FF}(f)$ (see Eq. (22)) is constructed from the proposed power spectra (Huang *et al*. 2014) and the empirical coherence functions (see Eq. (4), in which the exponential decay coefficient is 6.0) of the wind forces; the 'fitted coherence function-vortex shedding peak' means that the power spectra matrix $\boldsymbol{S}_{FF}(f)$ is constructed from the proposed power spectra and the coherence functions (see Eqs. (5) and (6), Eqs. (12) and (13), and Eqs. (15) and (16), considering the "head drop" at low frequencies) from which is subtracted the vortex shedding peak; the 'fitted coherence function' means that the power spectra matrix $\boldsymbol{S}_{FF}(f)$ is constructed from the proposed power spectra and the aforementioned coherence functions; and the "test results" means that the wind-induced responses are obtained directly by the aeroelastic model test.

Some conclusions are drawn from Fig. 29:

1. Comparison of the computed results by 'fitted coherence function-vortex shedding peak' method and 'fitted coherence function' method shows that for the X-axial (across-wind) displacement, the former was about 10% ~25% smaller than the latter; for the Y-axial (along-wind) displacement, there was little difference between the two; for the RZ-axial torsion angle, the former was slightly smaller than the latter. Comparing Figs. 6 to 8 shows the difference between the two mainly arose because the coherence functions along the X-axis and around the Z-axis had a peak near the vortex shedding frequency which did not occur along the Y-axis, moreover, the 1st torsional frequency was much larger than the 1st X-axial frequency.

2. The differences of displacement responses between 'empirical coherence function' method and 'fitted coherence function' method without vortex shedding peak were about 0%~10% or so, which reflected the influence of "head drop" effects of the coherence functions for the wind-induced responses of a high-rise building.

3. Overall considering of the analyses of points1 and 2, there exists about 0% ~30% error when using empirical coherence functions to construct the power spectra matrix to calculate structural responses for engineering application.

4. The vortex shedding frequency increased with the wind speed. When the wind speed reached 11.294 m/s, the vortex shedding frequency was close to the 1st structural frequency, which led to remarkable vortex-induced resonance with substantial increases in wind vibration response along the X-axis of nearly three times the normal values arising.

5. The results obtained by rigid model test differ from those obtained by aeroelastic model test with regards the influence of aerodynamic damping. Therefore, further research is deemed necessary.

6.2 Influence of load grouping and superposition method on wind-induced dynamic response

In practice, the random fluctuating wind loads acting on a building are commonly determined via a wind tunnel test of dynamic pressure measurement using a rigid model in conjunction with the pressure numerical integrating technique. For the purposes of promoting accuracy, both the number of pressure measurement layers along the height and the number of pressure measurement points on each layer should be sufficient. Strictly speaking, the random fluctuating wind loads on all measurement points of the rigid model should be synchronously measured. However, the pressure measurement in practice often has to be carried out group-by-group because of the large number of pressure measurement points and the limitation of the instrument capacity in channels of synchronous measurement, as shown in Fig. 2(b). In this case, the following strategy might be employed for estimating the structural responses.

Firstly, the pressure should be measured group-by-group from top to bottom along the height of the building, as shown in Fig. 2(b): the measurement points can be divided into four groups of A, B, C, and D or two groups of A and C.

Secondly, based on the proposed mathematical expressions of wind load (including power spectra and coherence functions), the responses of the building can be computed using the frequency domain method independently under the action of wind loads group-by-group corresponding to the grouping measurement of pressure.

Finally, the responses to the various groupings of wind loads can be combined using the Square Root of the Sum of Squares (SRSS) method discussed as follows.

Suppose that σ_{R_i} (i =1,…,N_G) is the standard deviation response to the i^{th} group of wind loads, then the total standard deviation response to all groups of wind loads can be expressed as

$$\sigma_R = \sqrt{\sum_{i=1}^{N_G} \sigma_{R_i}^2 + \sum_{i=1}^{N_G} \sum_{j=1, j\neq i}^{N_G} \sigma_{R_i R_j}} \tag{26}$$

where, N_G is the group number of wind loads (or pressure measurements); $\sigma_{R_i R_j}$ is the cross-covariance between the responses to the i^{th} and j^{th} groups of wind loads.

When the responses caused by all groups of wind load are completely correlated to each other, one has

$$\sigma_{R_i R_j} = \sigma_{R_i} \sigma_{R_j}, \quad \sigma_R = \sum_{i=1}^{N} \sigma_{R_i} \tag{27}$$

When the responses caused by all groups of wind load are completely uncorrelated to each other, one has

$$\sigma_{R_i R_j} = 0, \quad \sigma_R = \sqrt{\sum_{i=1}^{N} \sigma_{R_i}^2} \tag{28}$$

Actually, the responses to the different groups of wind loads are partially correlated. However, in light of previous experience, the correlation of wind loads on a building generally decreases fairly fast with the increase of distance. Therefore, if there is no overlap among the measurement regions of different groups, the wind loads acting on a layer within a region of one measurement group are less correlative to the others acting on the layers within different regions of other

measurement groups except that the wind loads acting on the layers within a narrow border zone of two neighboring measurement regions. Hence, if the group number of wind loads is small, the real total responses must be close to those calculated according to Eq. (28), i.e., the Square Root of Sum of Squares (SRSS) method, however, if the group number of wind loads become larger, they would be level off to those calculated according to Eq. (27), i.e., the direct superposition method.

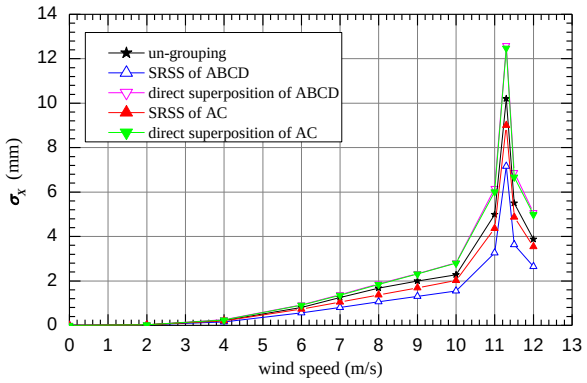

(a) along x axis

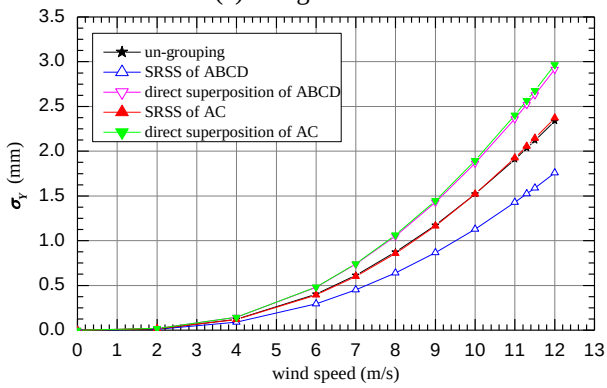

(b) along y axis

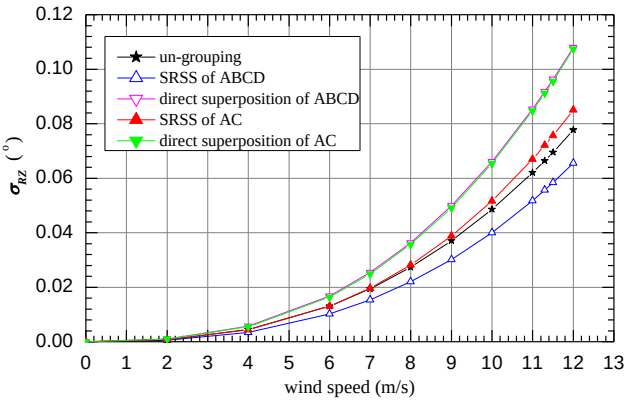

(c) around z axis

Fig. 30 Root of variances of displacement responses at top of building inwind direction 315°

Fig. 30 shows the root of the variances of the displacement responses at the top of building for 315° wind direction based on the frequency domain method and the proposed mathematical expressions of wind loads (including power spectra and coherence functions). In the figure, the un-grouping means that the power spectra matrix of wind loads is constructed from the proposed power spectra and coherence functions (see Eqs. (5) and (6), Eqs. (12) and (13), and Eqs. (15) and (16)), i.e., the aforementioned‘ fitted coherence function’ method; the SRSS of ABCD means that the wind-induced responses are calculated by SRSS method (see Eq. (28)), in which the response components respectively caused by groups A, B, C, and D wind loads are calculated by the frequency domain method based on the proposed mathematical expressions for the wind loads (including power spectra and coherence functions);the direct superposition of ABCD means that the wind-induced responses are calculated by direct superposition method (see Eq. (27)), in which the response components respectively caused by groups A, B, C, and D wind loads are calculated by the frequency domain method based on the proposed mathematical expressions of wind loads; the SRSS of AC means that the wind-induced responses are calculated by SRSS method (see Eq. (28)), in which the response components respectively caused by groups A and C wind loads are calculated by the frequency domain method based on the proposed mathematical expressions of wind loads; the direct superposition of AC means that the wind-induced responses are calculated by direct superposition method (see Eq. (27)), in which the response components respectively caused by groups A and C wind loads are calculated by the frequency domain method based on the proposed mathematical expressions of wind loads.

Some conclusions are drawn from Fig. 30:

1. The results calculated by the direct superposition of ABCD are similar to those from the direct superposition of AC, which means that the concentration of measurement points along height of such a building with section varying along height has little influence on the calculated wind-induced responses. It is obvious that the results calculated by the direct superposition method are an upper limit to the wind-induced responses.
2. The difference between the direct superposition of ABCD and the SRSS of ABCD is larger than that between the direct superposition of AC and the SRSS of AC, which means that the correlation of the responses caused by four groups of wind loads is weaker than that caused by two groups wind loads.
3. When the wind loads on the building are divided into two groups (A and C), the results by SRSS method are close to those found by un-grouping: they are slightly smaller along the X-axis and around the Z-axis, almost equal along the Y-axis.
4. When the wind loads on the building are divided into four groups (A, B, C, and D), the results by un-grouping are probably in between those of the SRSS method and direct superposition, therefore, the final wind-induced responses are best found by adopting the mean value of the results by the SRSS and the direct superposition methods.

7. Conclusions

Although the fitted parameters of mathematical expressions for coherence functions of wind loads vary from building to building, the type of mathematical expression and the inductive analysis method for summarizing the fitted parameters still have reference value on different buildings. Based on the proposed mathematical expressions of the power spectra and coherence functions, some analysis of wind-induced dynamic responses and the influence of the coherence

function, the load grouping and superposition method, and the contributions of turbulence force and vortex induced force, *etc*. were undertaken. Some conclusions can be drawn on the basis of the analysis of characteristics and mathematical expressions of the coherence functions of wind forces on super-tall buildings with sections varying along height, as well as the analysis of the effect of certain factors on the wind-induced dynamic responses:

(1) Overall, the correlations of wind forces at two positions weaken if their distances became larger. For the coherence functions of across-wind wind forces, peaks appear near the vortex shedding frequency, except those at the open edges of measurement levels. The coherence functions of along-wind wind forces basically follow an exponentially decaying trend, similar to that of the wind speeds themselves. The coherence functions of torsional wind forces are similar to those of their across-wind counter parts. Moreover, the coherence functions of wind forces as well as wind speeds exhibit a low frequency "head drop" effect.

(2) The mathematical expressions of coherence functions in across-wind and torsional-wind directions can be constructed by superposition of a modified exponential decay function and one or two peak functions caused by turbulent flow and vortex shedding respectively, while that in the along-wind direction need only be constructed by the former, similar to that of the wind speed.

(3) The top wind-induced displacement response of building in across-wind direction, considering the contribution of the vortex shedding peaks of coherence functions, was lager by about 10% to 25% than that un-considering. The top wind-induced displacement responses of building considering the "head drop" effects of coherence functions were larger or smaller about 0%~10% than that un-considering.

(4) The correlation of the responses caused by four groups of wind loads was smaller than that caused by two groups of wind loads. The results by SRSS method with two groups of wind loads, was more closer to the exact value than that by SRSS method with four groups of wind loads.

(5) When the turbulent force and vortex-induced force are separated to calculate the peak value responses of displacement in the across-wind direction, the result was smaller about 0% to 20% than that arising from their un-separated state when the vortex-induced resonance did not occur, it was smaller by about 50% in the face of vortex-induced resonance. When the vortex-induced resonance did not happen, the contribution for wind-induced responses mainly came from the turbulent forces. When vortex-induced resonance did occur, the contribution to the wind-induced responses mainly came from vortex-induced forces. When it was imminent but did not occur, the contributions of both the turbulent and vortex-induced forces to the wind-induced responses were significant.

Acknowledgments

The work described in this paper was supported by the National Natural Science Foundation (51208524), the Hunan Province Natural Science Foundation (12JJ4055), the Shanghai Education Committee Dawn Plan (04SG23), the Hunan Province University Innovation Platform Open Foundation(14k104), the China Postdoctoral Science Foundation (20100471227), and the Postdoctoral Science Foundation of Central South University. Any opinions and concluding remarks presented here are entirely those of the authors.

References

Davenport, A.G. (1965), "The relationship of wind structure to wind loading of Symposium", *Proceedings of the 3rd International Conference on Wind Effect on Building and Structures*. Vol.1, London.

ECCS Technical Committee T12 (1978), *Wind Effects, Recommendations for the Calculation of Wind Effects on Buildings and Structures*.

Gu, M. and Quan, Y. (2004), "Across-wind loads of typical tall buildings", *J. Wind Eng. Ind. Aerod.*, **92**(13), 1147-1165.

Hansen, S.O. and Krenk, S. (1999), "Dynamic along-wind response of simple structures", *J. Wind Eng. Ind. Aerod.*, **82**(1-3), 147-171.

Holmes, J.D. and Lewis, R.E. (1987), "Optimization of dynamics-pressure-measurement systems I. &II", *J. Wind Eng. Ind. Aerod*., **25**, 249-290.

Huang, D.M., Zhu, L.D. and Ding, Q.S. (2008), "Identification of modal parameters for a high-rise building aeroelastic model", *J.Vib. Eng.*, **21**(3), 291-297. (in Chinese)

Huang, D.M., Zhu, L.D. and Ding, Q.S. (2009), "Experimental research on vertical coherence function of wind velocities", *J. Exp. Fluid Mech.*, **23**(4), 34-40. (in Chinese)

Huang, D.M., Zhu, L.D. and Chen, W. (2014), "Power spectra of wind forces on a high-rise building with section varying along height", *Wind Struct.*, **18**(3), 295-320.

Irwin, H.P.A.H., Cooper, K.R. and Girard, R. (1979), "Correction of distortion effects caused by tubing systems in measurements of fluctuating pressures", *J. Wind Eng. Ind. Aerod*., **5**(1-2), 93-107.

Kareem, A. and Zhou, Y. (2003),"Gust loading factor - past, present and future", *J. Wind Eng. Ind. Aerod*,, **91**(12-15), 1301-1328.

Krenk, S. (1995), "wind field coherence and dynamic wind forces", *Symposium on the advances in Nonlinear Stochastic Mechanics*, (Eds., Noess and Krenk), Kluwer, Dordrecht.

Liang, S.G., Liu, S.C., Li, Q.S. Zhang, L.L. and Gu, M. (2002), "Mathematical model of acrosswind dynamic loads on rectangular tall buildings", *J. Wind Eng. Ind. Aerod.*, **90**(12-15), 1757-1770

Liang, S.G., Li, Q.S., Liu, S.C. Zhang, L.L. and Gu, M. (2004), "Torsional dynamic wind loads on rectangular tall buildings", *Eng. Struct.*, **26(1)**, 129-137.

Lin, N., Letchford, C., Tamura, Y., Liang, B. and Nakamura, O. (2005), "Characteristics of wind forces acting on tall buildings", *J. Wind Eng. Ind. Aerod*., **93**(3), 217-242.

Marukawa, H., Ohkuma T. and Momomura Y. (1992), "Acrosswind and torsional acceleration of prismatic high rise buildings", *J. Wind Eng. Ind. Aerod.*, **41-44**, 1139-1150.

Ministry of Construction P.R.China (2006), *Load code for the design of building structures-GB 50009-2006*, Chinese building industry press, Beijing, (in Chinese).

NIST HR-DAD, *high-rise database-assisted design*, http://www.itl.nist.gov/div898/winds/HR_DAD_RC_1.0/hr_dad_rc_1.0.htm

Shiotani, M. and Iwatani, Y. (1972), "Correlations of wind velocities in relation to the gust loadings", *Proceedings of the 3rd International Conference on Wind Effects on Buildings and Structures*, Saikon, Tokyo.

Simiu, E. and Scanlan, R.H. (1996), *Wind effects on structures*, 3rd Ed., Wiley, New York.

Simiu, E., Gabbai, R.D. and Fritz, W.P. (2006), "Wind-induced tall building response: a time-domain approach", *Wind Struct.*, **11**(6), 427-440.